AD-A113 659 SCHAFER (W J) ASSOCIATES INC WAKEFIELD MA F/G 20/5
LOW VOLTAGE FREE ELECTRON LASER OPTICS.(U)
MAR 82 N00014-80-C-0515
UNCLASSIFIED WJSA-FTR-82-193 NL

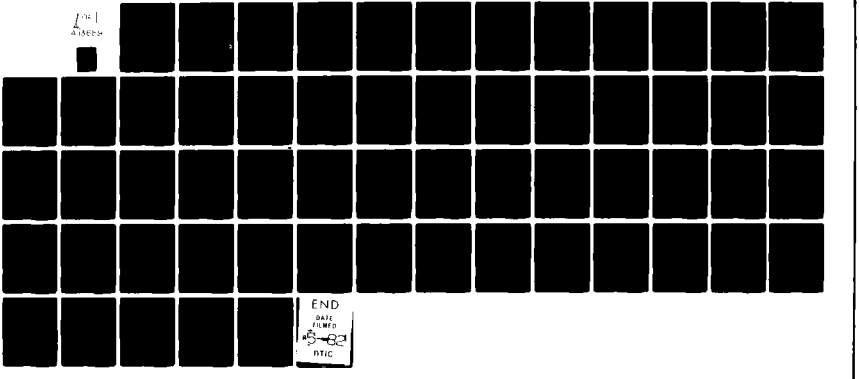

(2)

WJSA-FTR-82-193

LOW VOLTAGE FREE ELECTRON LASER OPTICS

5 March 1982

Contract Number: N00014-80-C-0515

Prepared for:

PCO - Office of Naval Research
Department of the Navy
800 N. Quincy Street
Arlington, VA 22217

Prepared by:

W. J. Schafer Associates, Inc.
10 Lakeside Office Park
Wakefield, MA 01880

(2)

WJSA-FTR-82-193

LOW VOLTAGE FREE ELECTRON LASER OPTICS

5 March 1982

Contract Number: N00014-80-C-0515

Prepared for:

PCO - Office of Naval Research
Department of the Navy
800 N. Quincy Street
Arlington, VA 22217

Prepared by:

W. J. Schafer Associates, Inc.
10 Lakeside Office Park
Wakefield, MA 01880

TABLE OF CONTENTS

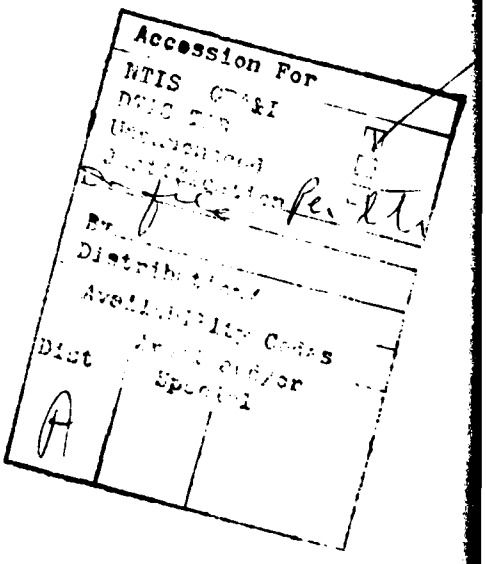

LIST OF FIGURES

LIST OF FIGURES (CONTINUED)

LIST OF TABLES

SECTION I

INTRODUCTION

During the past three years, we have been studying the applications of free electron lasers for Navy missions as well as the physics and technical issues of the low voltage free electron lasers. By low voltage we imply electron beams of kinetic energy < 10 MeV. In these devices the conventional magnetostatic wiggler is replaced by an electromagnetic pump of wavlength < 1 mm to generate doppler shifted coherent radiation in the visible portion of the electromagnetic spectrum. In our last study, we found that the extraction efficiency and available power with an electromagnetic pump depend critically on the emittance of the electron beam. We found further that the losses in the optical cavity of the pump beam must be $\leq 10^{-4}$ per round trip if the overall system efficiency is to be acceptable.

In this study, we look at several methods of reducing electromagnetic pump optical cavity losses. The only technology that seems to show any promise of being able to achieve the required low optical losses is the use of superconducting cavity. Even here there are physics and technology limitations. In general the system works better at pump wavelengths > 1 mm. In Section II, we summarize the results of the systems requirement analyses on cavity optics for the two stage FEL. In Section III, we discuss in detail the several methods suggested for decreasing cavity losses. Section IV contains several design maps for choosing the optical parameters of the system. The section contains a summary of parameters for a point design which is geared to the near term experiment of UCSB. Section V is a summary of the optical analysis reported with conclusions and recommendations.

SECTION II

OPTICAL CAVITY REQUIREMENTS

In this section, we summarize the results obtained by us in the previous study[3]. It has been shown that the constant parameter magnetostatic wiggler can result in an energy extraction of ~ 1/2 N per pass where N is the number of periods provided the FEL is homogeneously broadened. For the case of inhomogeneous broadening, the extraction efficiency is even lower. To improve the extraction efficiency in a single pass, it was proposed to vary the parameters of the wiggler in such a way that the ponderomotive potential well in which the electrons move is decelerated and, thereby, decelerating the electrons. In a magnetostatic wiggler, both the period, as well as the wiggler magnetic vector potential, can be designed to vary in a prescribed manner. However, with an electromagnetic pump of wavelengths less than 1 mm, first, the pump vector potential is too small to contribute significantly to the resonance condition; and secondly, it is not possible to change the wavelength of the pump. It has been suggested that the electron beam can be made to interact at varying interaction angle to the pump radiation (instead of π radians) such that the effective pump wavelength is altered. Such a scheme, though attractive, would severely restrict the interaction length. An alternate (and more practical) scheme is to use an axial accelerating field to keep the electrons at resonant energy and to keep them trapped in the ponderomotive potential well. For effective trapping, the electrostatic coulomb force between the electrons has to be much smaller than the attractive ponderomotive

potential force. In this regime of operation, then, single particle physics is applicable.

Neglecting the energy supplied by the accelerating field, the extraction efficiency is given by

$$\eta_{ext} = \frac{I_{ext}}{(\gamma - 1)\, mc^2\, J_{eb}} \tag{2.1a}$$

$$= \frac{2.68 \times 10^{-42}\, P_p^3\, \lambda_{p\mu}\, \lambda_{s\mu}^4\, L}{(\gamma - 1)\, \alpha^8\, C_c^3\, J_{eb}} \tag{2.1b}$$

where P_p is the pump power in watts, $\lambda_{p\mu}$ and $\lambda_{s\mu}$ are the pump and output wavelengths in microns, L is the interaction length in cm, J_{eb} is the current density in amp/cm^2, C_c is the out-coupling coefficient and α is the factor that determines beam quality.

In Figure (1), the extraction efficiency is plotted as a function of pump power for various values of the parameter α while fixing the equivalent spread due to emittance at 0.1%. This meant fixing $\alpha^2 j_{eb}$ at $\sim$ 64 amp/cm^2. The figure also points out the important gain that can be achieved in improving the beam emittance. The horizontal hatched line indicates a trapped fraction of 40% which is about the maximum that one can achieve in a nonadiabatic accelerating field. This is also the cold beam limit.

The overall system efficiency of a low voltage free electron laser that utilizes an electromagnetic pump can be written as

$$\eta_{sys} = \frac{\eta_c\, E_{acc}\, L\, I}{(1-\eta_R)\, I\, [\, (\gamma-1)mc^2 + (1-\eta_c)\, E_{acc} L\,] + \eta_c\, E_{acc}\, L\, I + \beta\, P_p/\eta_p} \tag{2.2}$$

where η_R is the recovery efficiency of the electron beam energy, β is the round trip fractional loss of the pump beam and η_p is the

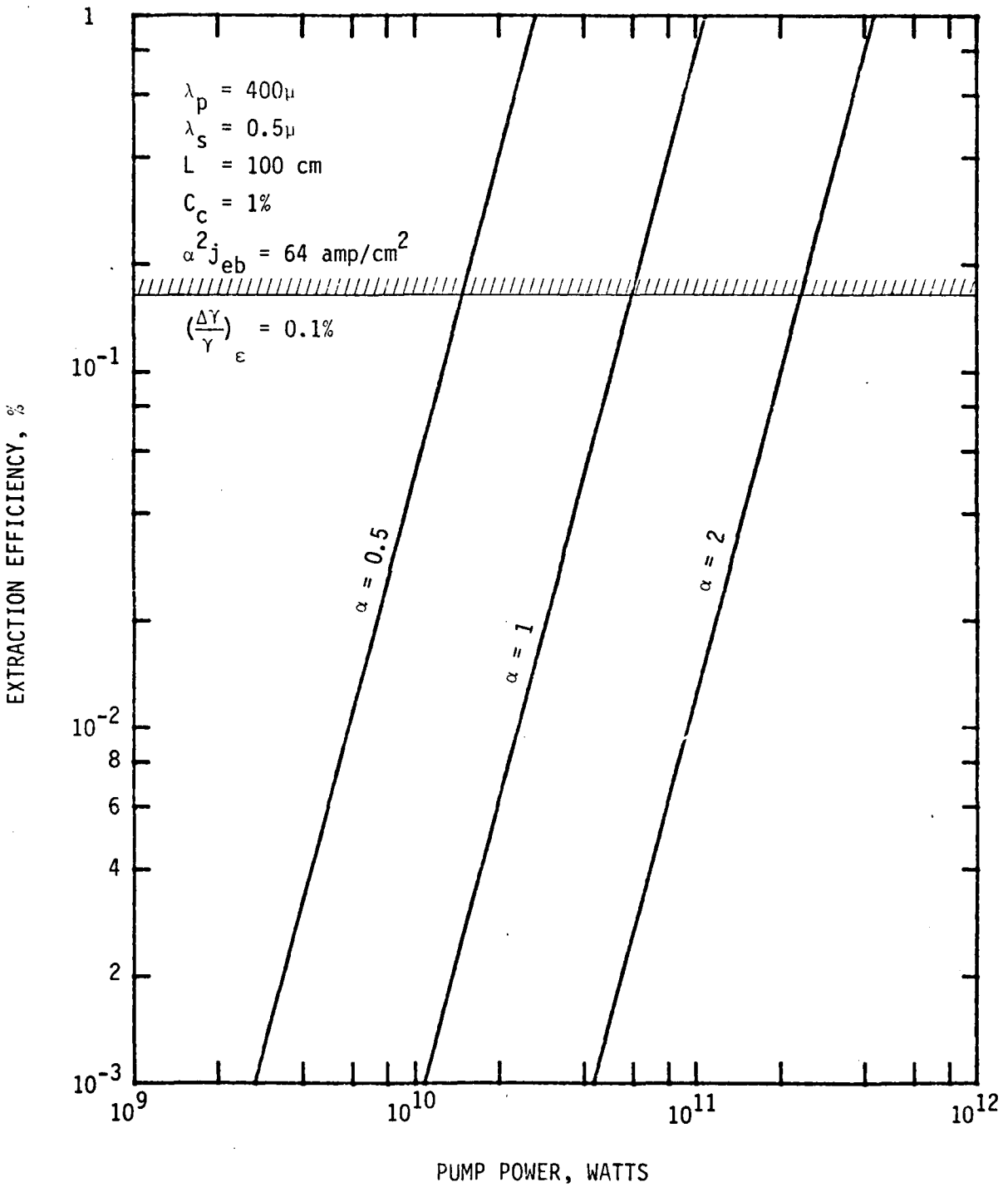

Figure 1. Effect of Emittance on Extraction Efficiency

efficiency of the pump laser system. In Figures 2 and 3, we have plotted the system efficiency versus β for a representative set of parameters with P_p as the third variable. It is clear from the figure that for devices of interest to Navy (medium to high powers) that the round trip losses of the pump beam must be less than 10^{-3} for any reasonable system efficiency. We are thus forced to design reflective optics for the pump cavity with > 99.9% reflectance per surface.

For output powers in excess of tens of kilowatts in the visible/-near IR, the circulating pump power required is in excess of 10^{10} watts, while the circulating power at the short wavelength would be in excess of 10^6 watts. One is then faced with the problem of designing and developing optical cavities at two disparate wavelengths with high to very high reflectivity at both the wavelengths. The optical design could be somewhat simplified if means can be found for separating the two wavelengths so that one can concentrate on the design of high reflectivity optics at a single wavelength.

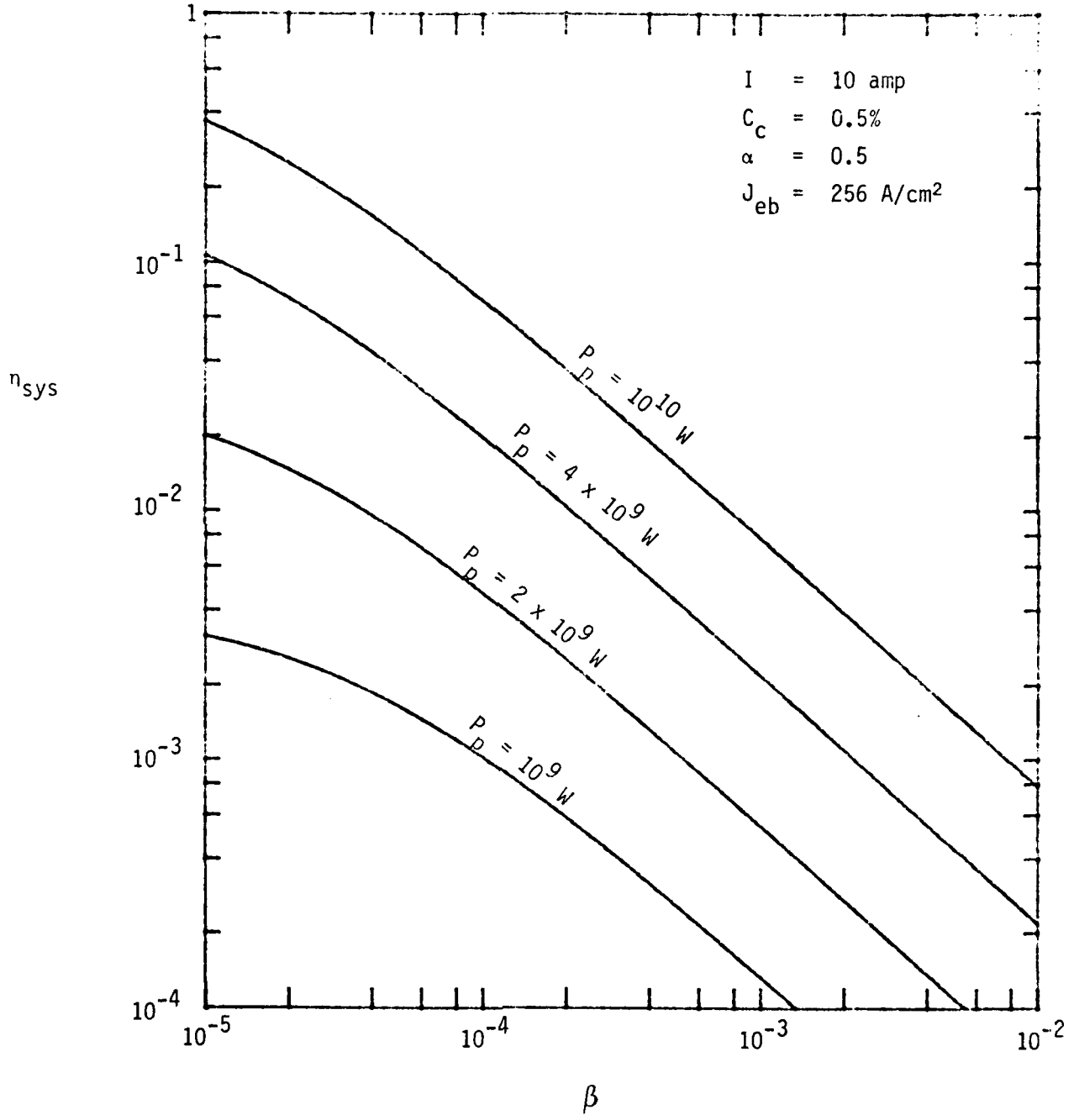

Figure 2. System Efficiency vs. Pump Cavity Loss at Moderate Current

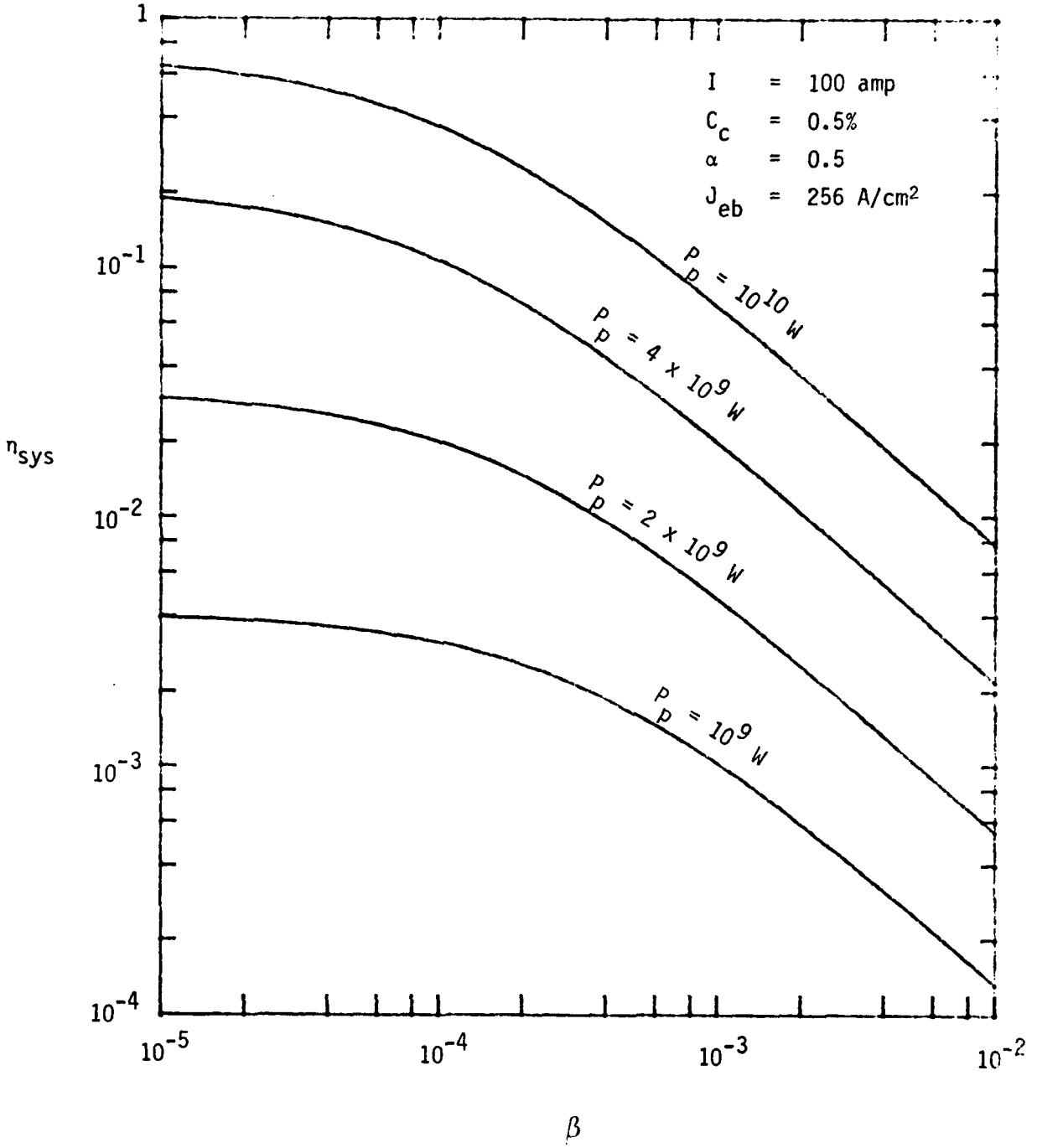

Figure 3. System Efficiency vs. Pump Cavity Loss at High Current

SECTION III

LOW LOSS CAVITIES

3.1 Room Temperature Metal Reflectors

The losses in an electromagnetic cavity can be classified as (i) absorption losses on the cavity walls, (ii) diffraction losses in open cavities and (iii) out coupling losses. The diffraction losses can be almost completely eliminated by going to closed cavities (save for letting e-beam in and out). However, as we shall see later, even in open resonators, they can be kept at 10^{-4} to 10^{-5} per round trip and thus would not pose significant problems. The out coupling losses come about because the output radiation at the short wavelength has to be coupled out and the pump radiation will leakout at this place. By the proper choice of the transverse cavity mode, this can be minimized. The most significant loss then would be the absorption loss on the cavity wall itself. In this section, we shall assess the possible methods of minimizing the absorption loss based on (a) material property and (b) on the geometry of the reflecting surface.

With conventional mirrors, one can consider (a) pure metallic conditions and (b) dielectric coatings for increasing the reflectivity. For good conductors, the surface resistance R_s can be written as[4]

$$R_s = 1/\sigma\delta \tag{3.1}$$

where σ is the conductivity and δ is the skin depth. The skin depth d is given by

$$\delta = (2/\omega\sigma\mu)^{1/2} \tag{3.2}$$

where ω is the frequency of the wave and μ is the permeability of the metal. The absorption loss at the surface of the metal can then be written as

$$\alpha_L = R_s/Z_o \qquad (3.3)$$

where Z_o is the free space impedence (377 ohms). Table I gives the surface resistance, skin depth and loss factor for different metals at 500 μ and 1000 μ. The loss factor α_L given in the table should be multiplied by 2 to obtain β for the cavity since two surfaces are involved. From this, we find that the best that one can achieve in the 500 to 1000 μ wavelength range is to have a round trip absorption loss of 0.1%. The values calculated in Table I are based on the assumption of idealized surface conditions. Surface contamination and imperfections on grain boundaries typically increase the absorption by a factor of 2.

The dielectric coatings, while increasing reflectivity significantly in the visible, do not offer the same advantage in the far infrared. In practice it is very difficult to improve over the reflectivity of silver[5]. The only problem with silver seems to be the oxide formation on the surface (tarnishing). Workers in the field prefer gold plated mirrors to silver for this reason. However, for the applicaton that we have in mind, silver would seem to be the best choice.

3.2 Reflection of an Electromagnetic Plane Wave by an Infinite Set of Parallel Wires

In this section we discuss the possibility of decreasing the mirror losses by replacing it with a set of parallel wires spaced less than $\lambda/2$ apart. Such an array of wires or tubes is frequently used in the microwave region to attenuate waves passing through such a structure. The configuration that we have in mind is shown in Figure 4.

TABLE I

ABSORPTION LOSSES ON THE SURFACE OF GOOD CONDUCTORS

Conductor	Conductivity σ mho/meter	λ = 500 μ			λ = 1000 μ		
		Skin depth δ, m	Surface Resistance R_s, ohm	Loss Factor α_L	Skin depth δ, m	Surface Resistance R_s, ohm	Loss Factor α_L
Aluminum	3.54×10^7	1.1×10^{-7}	0.26	6.9×10^{-4}	1.54×10^{-7}	0.18	4.9×10^{-4}
Copper	5.8×10^7	0.8×10^{-7}	0.20	5.36×10^{-4}	1.21×10^{-7}	0.14	3.79×10^{-4}
Silver	6.15×10^7	0.83×10^{-8}	0.196	5.21×10^{-4}	1.17×10^{-7}	0.139	3.68×10^{-4}
Gold	4.5×10^{-8}	0.97×10^{-8}	0.23	6.09×10^{-4}	1.37×10^{-7}	0.16	4.3×10^{-4}

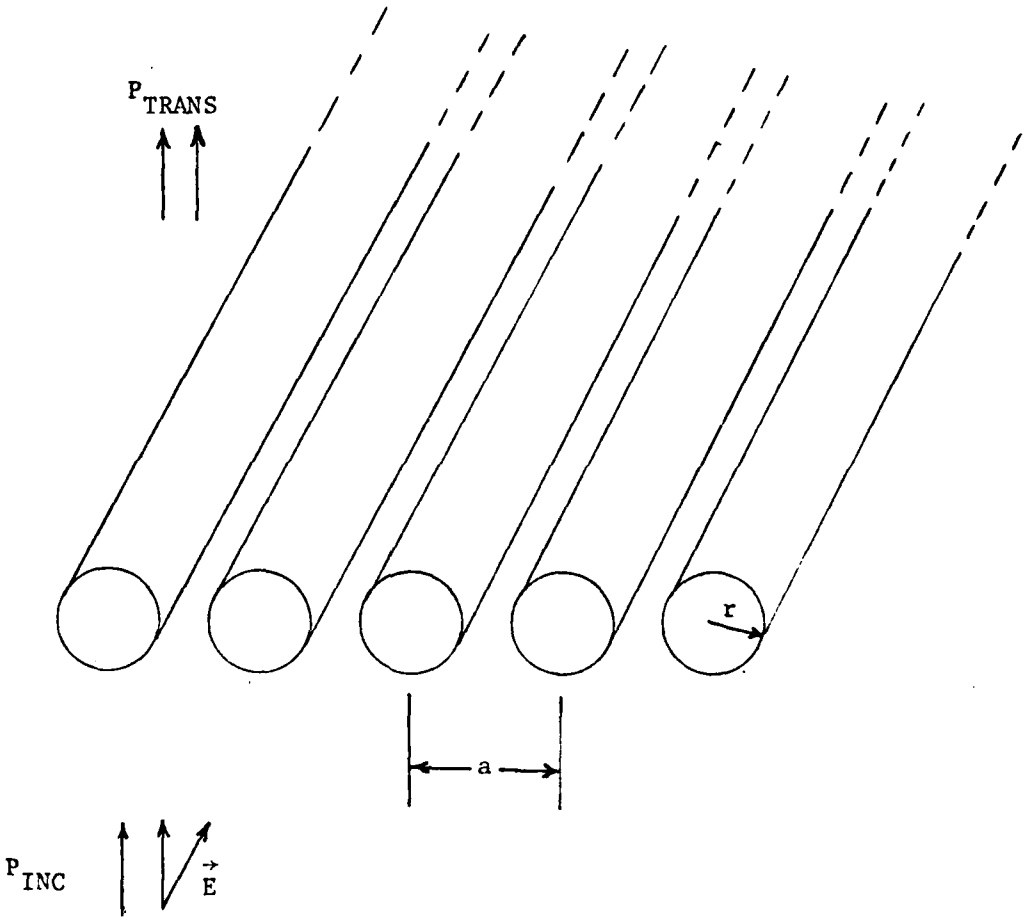

Figure 4. Geometry of Transmission through Parallel Wires

Mumford[6] has given an emperical formula for the ratio of incident to transmitted power (P_I/P_T) for such a geometry.

$$\frac{P_I}{P_T} = \frac{B^2}{4} \tag{3.4}$$

where

$$|B| = \frac{\lambda}{a} \Big/ \ln \left[\frac{0.83 \exp (2\pi r/a)}{\exp (2\pi r/a) - 1} \right] . \tag{3.5}$$

The electric field vector is parallel to the direction of the wires and the propagation direction is normal to the plane of the wires. This relationship is shown plotted in Figure 5 for several values of the ratio a/2r. A word of caution is in order about equation (3.5). It does not go to the right limits when a→2r. This is to be expected since equation (3.5) is only an empirical fit, but the author claims an accuracy of 1 db over interesting ranges of a/2r (i.e. from 3 to 30). In order to show significant improvements over commercially available mirrors one would like to have $P_{inc}/P_{Trans} \gtrsim 10^4$. One would also like to have a/2r as large as possible since the formula doesn't include absorption losses by the wires. Fabrication technology would limit the smallness of the radius of the wires. Table II gives the wire diameter necessary to achieve a transmission loss of 40 db for different values of a/2r. Whether this would be possible remains to be seen. In addition, the fluence level that can be withstood by the wires would be significantly lower than that for the plane mirror which can be cooled more easily. We are therefore forced to conclude that this may not be a practical approach to making high reflectivity cavities.

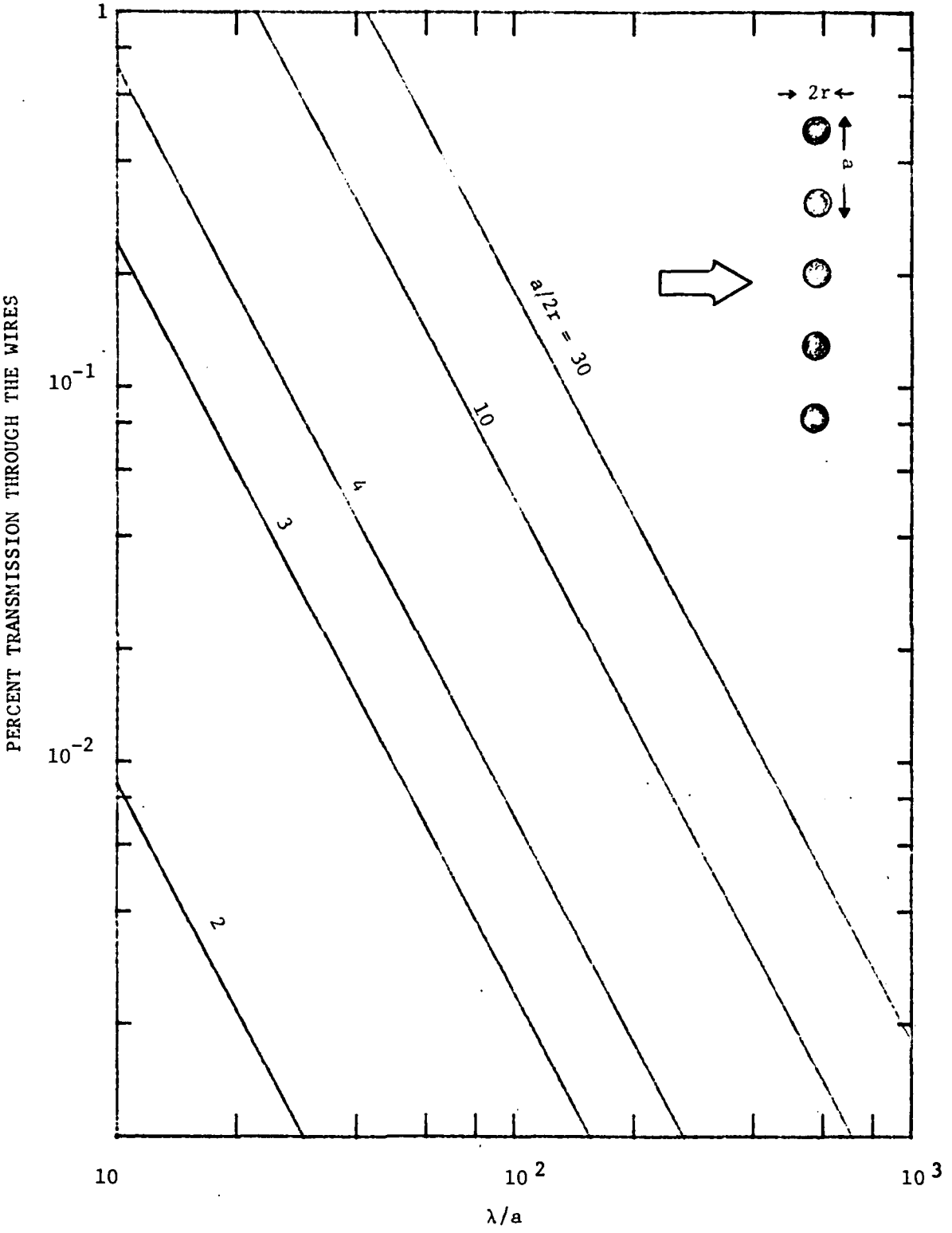

Figure 5. Percentage Transmission through Parallel Wires

TABLE II

WIRE DIAMETERS CORRESPONDING TO $P_{INC}/P_{TRAN} = 10^4$

λ μm	a/2r	Diameter = 2 r μm
1000	3	6.8
1000	4	3
1000	10	0.44
500	3	3.4
500	4	1.5
500	10	0.22

3.3 Reflection of an Electromagnetic Plane Wave By an Infinite Set of Plates

It has also been suggested that the losses in a plane mirror can be reduced by changing the geometry to a set of parallel plates spaced $< \lambda/2$ apart such that waves with electric field vector polarized parallel to the plates cannot propagate inside the plates (evanescent wave only). This geometry is illustrated in Figure 6. For the case of perfect conductor, the set of plates act as perfect plane mirror. In the case of a good conductor, the hope was that the absorption losses would be significantly reduced from that of the plane mirror because of the geometrical reduction in the area of the arrays normal to the direction of incidence of the electromagnetic wave. In this section, we shall, however, prove that this is not the case. When $\lambda < 2a$ where a is the separation distance between the plates, significant amount of field is set-up between the plates even though it decays with distance. The surface current set-up by this field actually causes more power to be dissipated than in the case of a plane mirror.

The problem of the field distribution when a plane electromagnetic wave is incident upon an infinite set of staggered, equally spaced, semi-infinite metallic plates of zero thickness and perfect conductivity was solved in a set of papers by Carlson and Heins in 1947. The boundary value problem for the field was formulated mathematically as Weiner-Hopf integral equation and a rigorous solution to the integral equation was obtained by Carlson and Heins by Fourier transform techniques. An expression for the surface current density and hence the field was obtained in the Fourier transform domain. The actual

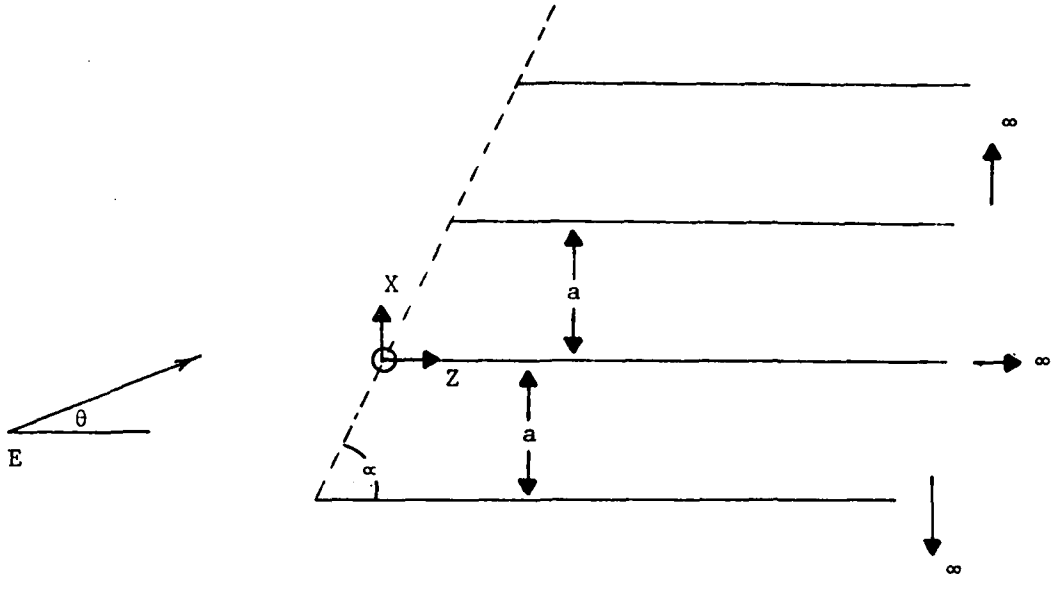

Figure 6. Geometry of an Array of Parallel Plates

inversion of this transform to the physical space was not carried out by the authors. Nevertheless, they were able to obtain asymptotic expression for the reflected and transmitted fields. We are however able to use their results and obtain closed form expression for the power dissipated in such an array of plates when we relax the infinite conductivity requirement. The current density J in a good conductor is confined to such a small thickness just below the surface of the conductor that it is equivalent to an effective surface current K_{eff}:

$$K_{eff} = \int_0^\infty J \, d\xi = \vec{n} \times \vec{H}_{\parallel} \qquad (3.6)$$

where ξ is the distance into the conductor and $H_{\parallel}$ is the parallel component of the magnetic field[4]. Comparison of equation (3.6) with a similar one for the perfect conductor shows that a good conductor behaves effectively like a perfect conductor, with the idealized surface current replaced by an equivalent surface current which is actually distributed throughout a very small, but finite, thickness at the surface. The power loss per unit area can be written in terms of the effective surface current:

$$\frac{dP_{loss}}{dA} = \frac{1}{2\sigma\delta} |K_{eff}|^2 \qquad (3.7)$$

where σ is the conductivity of the metal and δ is the skin depth. Thus, if we have solved for the field and currents for the idealized problem of infinite conductivity, we can calculate approximately the absorption losses for the non-ideal conductor.

In what follows, we shall be concerned only with the case of polarization such that the electric field vector is parallel to the plates. In the case when the H-field is parallel to the plates, the

fundamental mode can be sustained for propagation between the plates and hence is not of interest for the application that we are discussing here. When the E-field is parallel to the plates, all the field components can be derived from $\phi\ (x,z) = E_y\ (x,z)$.

Carlson and Heins[7] define a quantity $I_m(z)$ which is proportional to the surface current density K(z) on the mth plate. We are interested in the case when the angle $\alpha = \pi/2$ and the angle of incidence $\theta = 0$. From Reference 7, we have

$$J\ (w) = \frac{2\ i\ K_+\ (k \cos\ \theta)}{K_-\ (w)\ (w-k \cos\ \theta)} \tag{3.8}$$

where J(w) is the Fourier transform of $I_o(z)$ and w is the transform variable. The functions $K_+\ (w)$ and $K_-\ (w)$ are given by

$$K_+(w) = \frac{(a^2 + b^2)(w-\sigma_2)\ \exp\ [\ \chi\ (w)]\ G_1\ G_2}{2a\ G_3\ (w + \kappa)\ \exp\ (iaw/\pi)} \tag{3.9}$$

$$K-(w) = \frac{G_4\ \ (w-\kappa)\ \exp\ [\ -iaw/\pi + \chi\ (w)]}{(w-\sigma_1)\ G_5\ G_6} \tag{3.10}$$

where

$$G_1 = \prod_{n=1}^{\infty} [\Delta_n - i\psi_n] \exp\ \{[k\rho\_wb+wai)/2\pi n]+i(\pi/2-\alpha)\}$$

$$G_2 = \prod_{n=-\infty}^{-1} [\Delta_n + i\psi_n]\ \exp\ \{\ [(k\rho-wb+wai)/2\pi n]-i(\pi/2-\alpha)\}$$

$$G_3 = \prod_{n=2}^{\infty} \left[\ \sqrt{1 - \left(\frac{ak}{\pi n}\right)^2} - \frac{iaw}{\pi n}\ \right] \left(\frac{a}{\pi}\right) \exp\ [iaw/n\pi]$$

$$G_4 = \prod_{n=2}^{\infty} \left[\ \sqrt{1 - \left(\frac{ak}{\pi n}\right)^2} + \frac{iaw}{\pi n}\ \right] \frac{a}{\pi} \exp\ (-iaw/\pi n)$$

$$G_5 = \prod_{n=-\infty}^{-1} [\Delta_n - i\psi_n]\ \exp\ \{[(k\rho-wb+wai)/2\pi n] + i(\pi/2-\alpha)\ \}$$

$$G_6 = \prod_{n=1}^{\infty} [\Delta_n + i\psi_n] \exp \{[(k\rho - wb - wai)/2\pi n] - i(\pi/2 - \alpha)\}$$

$$\sigma_1 = k \cos \theta, \quad \sigma_2 = k \cos (2\alpha - \theta),$$

$$\Delta_n = \sqrt{\sin^2 \alpha \left(1 - \frac{k\rho}{2\pi n}\right)^2 - \left(\frac{ak}{2\pi n}\right)^2}, \quad \psi_n = \cos \alpha \left(1 - \frac{k\rho}{2\pi n}\right) + \frac{wa \csc \alpha}{2\pi n}$$

$$b = a \cot \alpha, \quad \rho = b \cos \theta + a \sin \theta$$

$$\chi(w) = \frac{-iaw}{\pi} \left[\left(\alpha - \frac{\pi}{2}\right) \cot \alpha - \ln 2 \sin \alpha \right]$$

Since the surface current density on the plates is a function of distance into the plates, we are really interested in

$$\int_0^{\infty} |K(z)|^2 \, dz = \frac{1}{k^2} \int_0^{\infty} |I_o(z)|^2 \, dz. \tag{3.11}$$

The quantity $I_o(z)$ is defined to be identically zero for $z < 0$.

Therefore, we can use Parseval's formula and write

$$\int_0^{\infty} |I_o(z)|^2 \, dz = \int_{-\infty}^{\infty} |I_o(z)|^2 \, dz = \int_{-\infty}^{\infty} |J(w)|^2 \, dw \tag{3.12}$$

For the special case of $\alpha = \pi/2$ and $\theta = 0$, we find that

$$|K_+(k)|^2 = k^2 a^2 \text{ and}$$

$$|K_-(w)(w-k)|^2 = - \prod_{n=1}^{\infty} \frac{\left[1 - \left(\frac{ka}{\pi n}\right)^2 + \left(\frac{wa}{\pi n}\right)^2\right]}{\left[1 - \left(\frac{ka}{2n\pi}\right)^2 + \left(\frac{wa}{2n\pi}\right)^2\right]^2}$$

We therefore have,

$$\int_{-\infty}^{\infty} |J(w)|^2 \, dw = -4 k^2 a \int_{-\infty}^{\infty} d\xi \prod_{n=1}^{\infty} \frac{[1 - (\mu/n)^2 + {}^2(\xi/n)^2]}{[1 - (2\mu/n)^2 + (2\xi/n)^2]} \tag{3.13}$$

where

$\xi = wa/2\pi$ and $\mu = ka/2\pi = a/\lambda$.

The integral can be evaluated by the method of residues. The poles of the integrand are located at

$$\xi = \pm i \xi_n = \pm i \sqrt{n^2/4 - \mu^2} \qquad (\mu < 1/2). \tag{3.14}$$

Evaluating the residues, we have,

$$\int_{-\infty}^{\infty} |J(w)|^2 \, dw = 4k^2 a \sum_{m-1}^{\infty} \frac{\prod_{n=1}^{\infty} (1-m^2/4n^2)^2}{\prod_{\substack{n=1 \\ n\neq m}}^{\infty} (1-m^2/n^2)^2 \sqrt{m^2/4-\mu^2}} \tag{3.15}$$

The infinite products can be written in terms of simple trigonometric functions and the final result is,

$$\int_{-\infty}^{\infty} |J(w)|^2 \, dw = \frac{64}{\pi} k^2 a \sum_{p=0}^{\infty} (2p+1)^{-2} [(2p+1)^2 - 4\mu^2]^{-1/2} \tag{3.16}$$

The power loss per sheet per unit distance in the y-direction is therefore given by

$$\frac{dP_{sheet}}{dy} = \frac{a}{2\sigma\delta} \cdot \frac{64}{\pi} |H|^2 \sum_{p=0}^{\infty} (2p+1)^{-2} [(2p+1)^2 - 4\mu^2]^{-1/2} \tag{3.17}$$

In the case of a plane mirror, the effective surface current is

$$|K_{eff}| = |\vec{n} \times \vec{H}|. \tag{3.18}$$

The power loss in plane mirror per unit distance in the y-direction and distance a in the n direction is

$$\left.\frac{dP}{dy}\right|_{\text{plane mirror}} = \frac{a}{2\sigma\delta} |H|^2 \tag{3.19}$$

Comparing Equation (3.17) and (3.19), we can find the ratio of power loss with a stack of sheet to that of the plane mirror. If this ratio is described by R, we obtain,

$$R = \frac{64}{\pi} \sum_{p=0}^{\infty} (2p+1)^{-2} [(2p+1)^2 - 4\mu^2]^{-1/2} \qquad (3.20)$$

In Figure 7 we have plotted R vs μ (= a/λ). When $\mu \to 0$, we find that R tends to ~ 21.43 while $R \to \infty$ as $\mu \to 0.5$. The fact that R is not equal to 1 at $\mu = 0$ is not surprising since the theory was developed for sheets of zero thickness and we cannot, therefore, expect to recover the limit of plane mirror when the distance between the sheets approaches zero. In fact, we do not expect the results to be strictly valid when the distance between the plates is less than or comparable to the skin depth. The conclusion that we can obtain from Figure 7 is that the idea of using a stacked set of plates instead of a plane mirror will not result in reducing absorption losses; on the contrary, they will increase the total resistance losses.

3.4 Superconducting Cavities

3.4.1 Introduction

From the two preceding subsections, it is clear that the losses on the cavity walls cannot be decreased significantly (if at all) by purely geometrical means. The only other alternative to consider is the use of superconducting optics to reduce the losses significantly. There are two fundamental limits on the operation of the superconducting cavities. These are (i) the wavelength limit and (ii) the surface

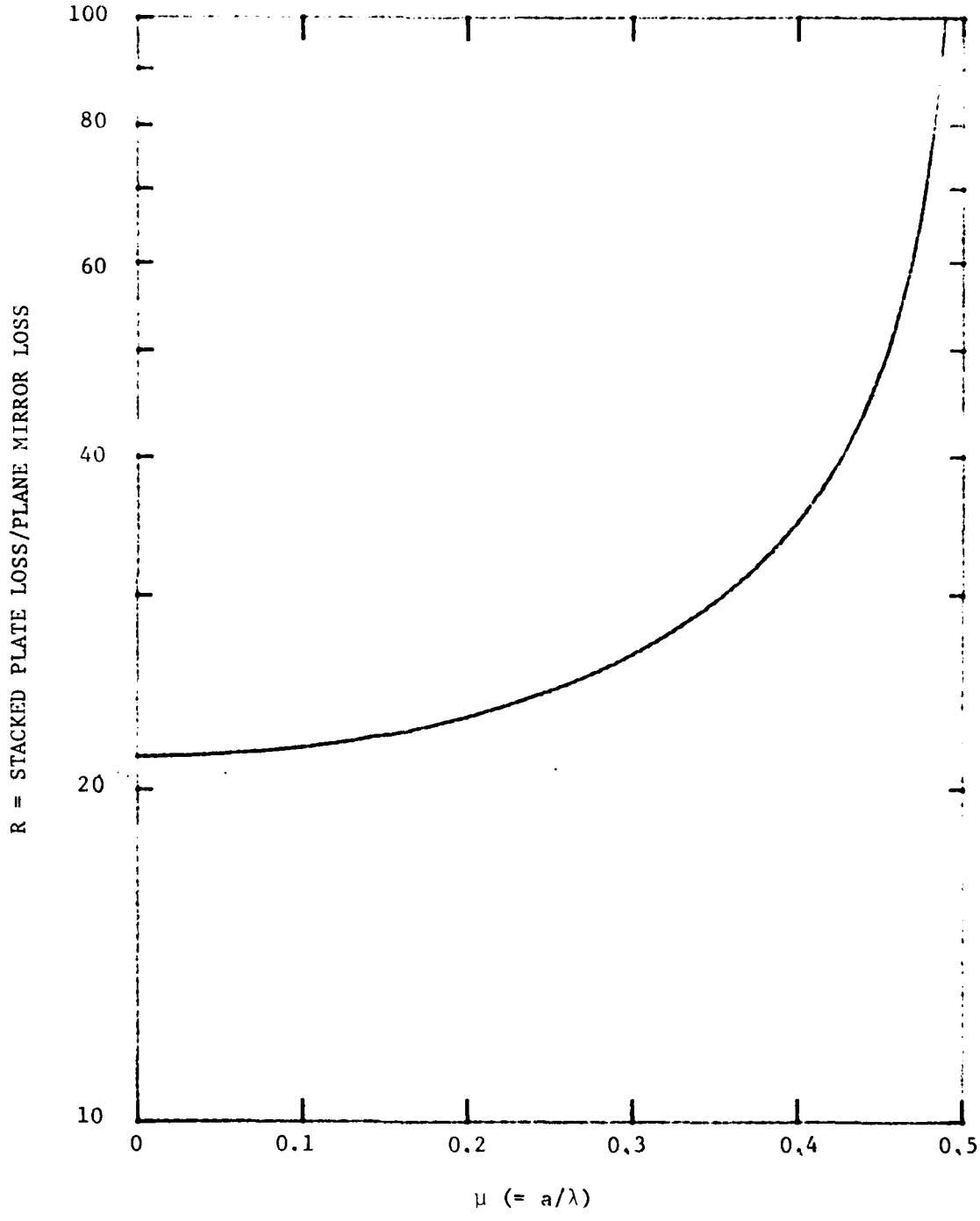

Figure 7. Ratio of Parallel Plate Loss to Plane Mirror Loss versus (a/)

magnetic flux density limit. The experimental data on the performance of the superconducting cavities lies mostly in the wavelength of a few centimeters while we are interested in millimeter and submillimeter wavelength region. Thus, caution must be exercised in using the extrapolated values of the surface resistance at these wavelengths.

In a superconductor the lowest excited state for an electron is separated by an energy gap Δ from the ground state. The existence of this gap in the excitation spectrum has been confirmed by a variety of experiments: electronic heat capacity, thermal conductivity, ultrasonic attenuation, far infrared and microwave absorption, and tunneling. It is to be noted that the excitation of electrons across the gap by photons requires a minimum energy of 2Δ, which is consistent with the description of the superconducting state in terms of Cooper pairs as described in Reference 9. The energy gap decreases monotonically with increasing temperature having a value $\Delta_0 \approx 1.75\ k\ T_c$ at 0°K and vanishing at the critical temperature T_c (where k is the Boltzmann constant).

Thus for frequencies ω at which the energy of the electrons $\hbar\omega$ is smaller than 2Δ, superconductivity can be achieved. This accounts for the fact that at D.C. and low frequencies superconductivity can be achieved at temperatures very little below T_c. To operate at higher frequencies the gap Δ must be increased.

The limiting frequency f at 0°K for Niobium is 717 GHz ($T_c \approx 9.25$°K) while for Niobium Tin it is 1395 GHz ($T_c \approx 18$°K).

At temperatures above 0°K the limiting frequency decreases to zero monotonically. No simple relationship for the decrease seems to exist.

It is probably reasonable to assume as a first estimate that one should divide the values of $(f)_{0°K}$ by a factor of 2 for operating at a temperature above 0°K and another factor of 2 to provide a margin. This then would give the limits as

$f \approx 180$ GHz or $\lambda = 1667$ micrometer for Niobium

$f \approx 349$ GHz or $\lambda = 860$ micrometer for Niobium Tin

If the total dividing factor of 4 is too large it may be possible to reach somewhat shorter wavelength.

The surface resistance of a superconductor has been theoretically derived to be equal to[10]

$$R_{BCS} \propto \frac{\omega^{1.7}}{T} \; e^{-\Delta(T)/kT}$$

where the subscript BCS refers to the Bardeen, Cooper and Schriefer theory. By fitting the experimental data to the theory, one finds that the actual relationship is

$$R_{BCS} = 2.4 \times 10^{-21} \times \frac{(2\pi f)^{1.7}}{T} \; e^{-1.86 \frac{T_c}{T}} \text{ OHMS} \qquad (3.21)$$

A complication arises due to the fact that there is a small residual surface resistance R_{RES} which must be added to R_{BCS} and presents a lower limit which is approached asymptotically as T approaches 0°K. It appears that this residual resistance is very much a function of surface preparation and condition. The residual resistance may also be a function of frequency especially when operating close to the wavelength limit discussed above.

In order to obtain a reasonable extrapclation to the wavelengths of interest based on the experimental data at 10 GHz = 30 mm in References 10, 11 and 12 we have used the $\omega^{1.7}$ scaling and these are shown in Table III.

It is seen in Table III that Niobium Tin at 4.2°K can reduce the loss factor by 2 to 3 orders of magnitude and Niobium at 1.5°K by about another order of magnitude as compared with copper at room temperature. The losses will in fact become so low that they will become negligible compared with the coupling, stray and diffraction losses. Note also that low losses make lower power demands on the cryogenic equipment and ease thermal conductivity oriented features. It is important to recognize that only if these other losses can also be kept low does it make sense to go to superconductors.

In addition to the wavelength limit, a limitation on the rf field strength of superconducting resonators exists and is given by the thermodynamically critical flux density B_c. For type I superconductors such as In.Sn and Pb with a low B_c, this limit is really observed. In type II superconductors external magnetic fields penetrate into the superconductor at the lower critical flux density B_{c1}, leading to hysteresis losses. According to more recent investigations, however, the value B_{c1} is not important at frequencies in the GHz range, so even with type II superconductors the rf field strength should be limited by B_c. In general, however, the measured rf field strengths are still below this limit.

Table 3 of Reference 10 shows a decrease in critical RF flux densities for Niobium cavities from 1000-1500 Gauss at 8.6 - 10.5 GHz

TABLE III

SURFACE RESISTANCE AND LOSS FACTORS FOR SUPERCONDUCTORS

Material	Operating Temperature	Wavelength = 1 mm		Wavelength = 400 μm	
		Surface Resistance r	Loss Factor β	Surface Resistance r	Loss Factor β
Niobium Tin T_c = 18° K	4.2° K	1.6×10^{-4}	8.6×10^{-4}	7.7×10^{-4}	4.1×10^{-6}
Niobium T_c = 9.25° K	1.5° K	8.1×10^{-6}	4.3×10^{-8}	3.85×10^{-5}	2.04×10^{-7}

to abcut 800 Gauss at 3.7 GHz 650-850 Gauss at 2.8 GHz and 350 Gauss at 1.3 GHz. For one of the data points the flux density observed exceeded the lower critical flux density B_{c1}. This confirms the above claim that the value B_{c1} is not necessarily limiting at frequencies in the GHz range. It remains to be seen if this trend continues to increase the critical flux for the higher frequencies of interst which would be useful in our application. We may take the maximum RF field on the surface of the superconductor to be ~ 1000 gauss which correspond to an intensity of ~ 10^8 w/cm^2 on the cavity walls. If the free electron laser requires an intensity of ~10^{10} w/cm^2 in the interaction region, the beam has to be expanded by a factor of 100 or greater in area before it hits the walls of the superconducting cavity.

The major problem with the operation of the superconducting cavity is the cryogenic power requirement. Typically, it takes 1 to 2 kilowatts of power to remove 1 watt of heat at 4°K. From the point of view of the overall system efficiency it then becomes clear that nothing would be gained by resorting to superconducting cavity if the losses are not decreased by more than three orders of magnitude compared with room temperature cavity. In addition to heat addition to the walls of the superconductor by the pump radiation, one also has to minimize radiational heating of the mirror by the ambient around the mirror. One would have to cool the entire FEL system by successive stages of cryogenic cooling. Our conclusion is thus that the superconducting cavity might work in a practical system if (i) the pump wavelength is greater than a few millimeters and (ii) the operating temperature is below ~ 2°K. Clearly, for the proposed UCSB experiment one would not want to complicate matters by using superconducting cavity.

SECTION IV

CAVITY DESIGN CONSIDERATIONS

From the preceding sections, we can conclude that for near term experiments the optical cavity in the far infrared is best fabricated using silver mirrors. For the demonstration of the concept of two-stage FEL, it is not necessary to have very high reflectivity. In this section, we shall map out the optical cavity parameters on a consistent set of axes. A number of assumptions will be made in deriving various formulae and these will be stated without always a complete justification.

We shall first assume that the first stage wiggler is made out of $SmCO_5$ permanent magnet as shown in Figure 8. For a magnet bar height $g = 3\ \lambda_w/8$ and a fill factor of unity, i.e. no gaps between neighboring magnets, the normalized wiggler vector potential on axis can be written[13]

$$a_w = 1.07 \times 10^{-4}\ B_r \lambda_w \exp\ [\ -\ 2\pi\ h/\lambda_w] \qquad (4.1)$$

where B_r is the remnant field in gauss and other quantities are defined in Figure 8.

The photon beam width at the entrance to the wiggler is denoted by 2w and for reasonable clearance the magnet separation 2h can be taken to be at least a factor of α larger than 2w. The Rayleigh range Z_R is related to the photon beam waist radius w_o by

$$Z_R = \pi\ w_o^2\ /\lambda \qquad (4\text{-}2)$$

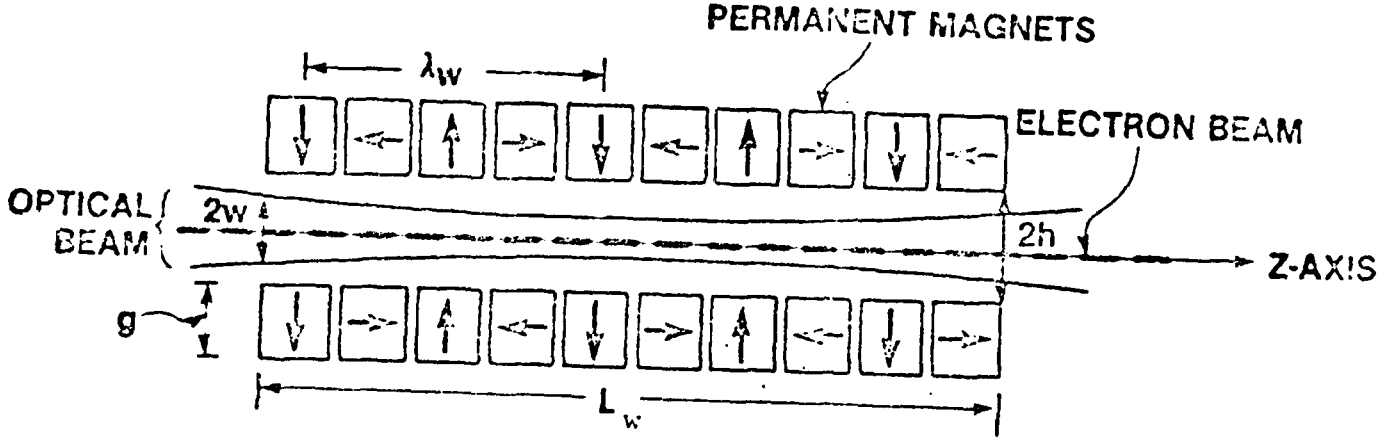

Figure 8. Geometry of the Permanent Magnet Wiggler for Optimization (From Ref. 13)

The length of the wiggler L_W is taken to be 2 q times the Rayleigh range. Thus the beam radius at the entrance to the wiggler can be written as

$$w = w_o \left[1 + \left(L_w/2Z_R \right)^2 \right]^{1/2}$$

$$= \left[\lambda Z_R \left(1 + q^2 \right)/\pi \right]^{1/2} \qquad (4.3)$$

Replacing h in equation (4.1) by αw and substituting (4.3) we get,

$$a_w = 1.07 \times 10^{-4} B_r \lambda_w \exp \left[-2\pi\alpha \left[\lambda Z_R (1 + q^2)/\pi \right]^{1/2}/\lambda_w \right] \qquad (4.4)$$

The output wavelength λ is related to λ_w and a_w through

$$\lambda = \lambda_w (1 + a_w^2)/2\gamma^2 \qquad (4.5)$$

The two convenient set of independent parameters are λ_w and Z_R and we shall plot the different physical quantities in maps with λ_w and Z_R as axes. Figures (9) and (10) show a plot of constant a_w lines. In plotting the figure, we had to assume a value for γ the electron beam energy. The maximum value of γ that can be obtained for the UCSB experiment is 12 and we have taken that to be a fixed value. Changing γ would result in similar plots.

The small signal gain $g_o L_w$ per pass is given by [14]

$$g_o L_w = \frac{2}{\pi} \frac{1}{\sqrt{e\pi}} \frac{r_o^2 n_e}{mc^2} \frac{B^2 \lambda_w^2}{(1 + a_w^2)^{1/2}} \frac{\lambda^{3/2}}{\lambda_w^{1/2}} \frac{L_w}{(\Delta\upsilon/\upsilon)^2} \qquad (4.6)$$

where r_o is the classical electron radius, n_e is the electron density in the beam and $(\Delta\upsilon/\upsilon)$ is the fractional line width and is taken to be ~ 1/2N (N being the number of wiggler periods). If we assume that the photon beam waist radius and electron beam radius are matched, equation (4.6) can be rewritten as

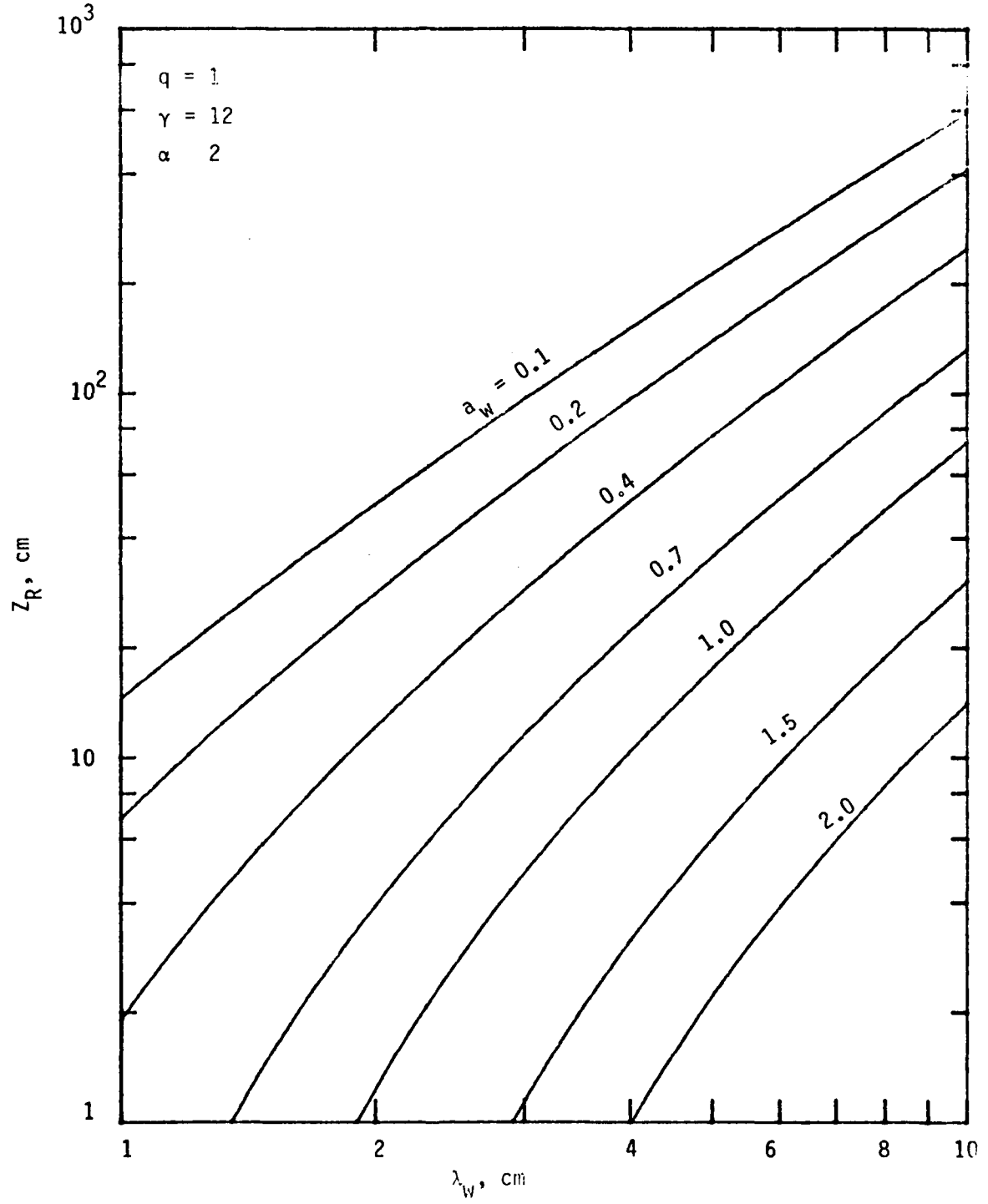

Figure 9. Map of Constant a_w Lines for a Permanent Magnet Wiggler in λ_w - Z_R Parameter Space

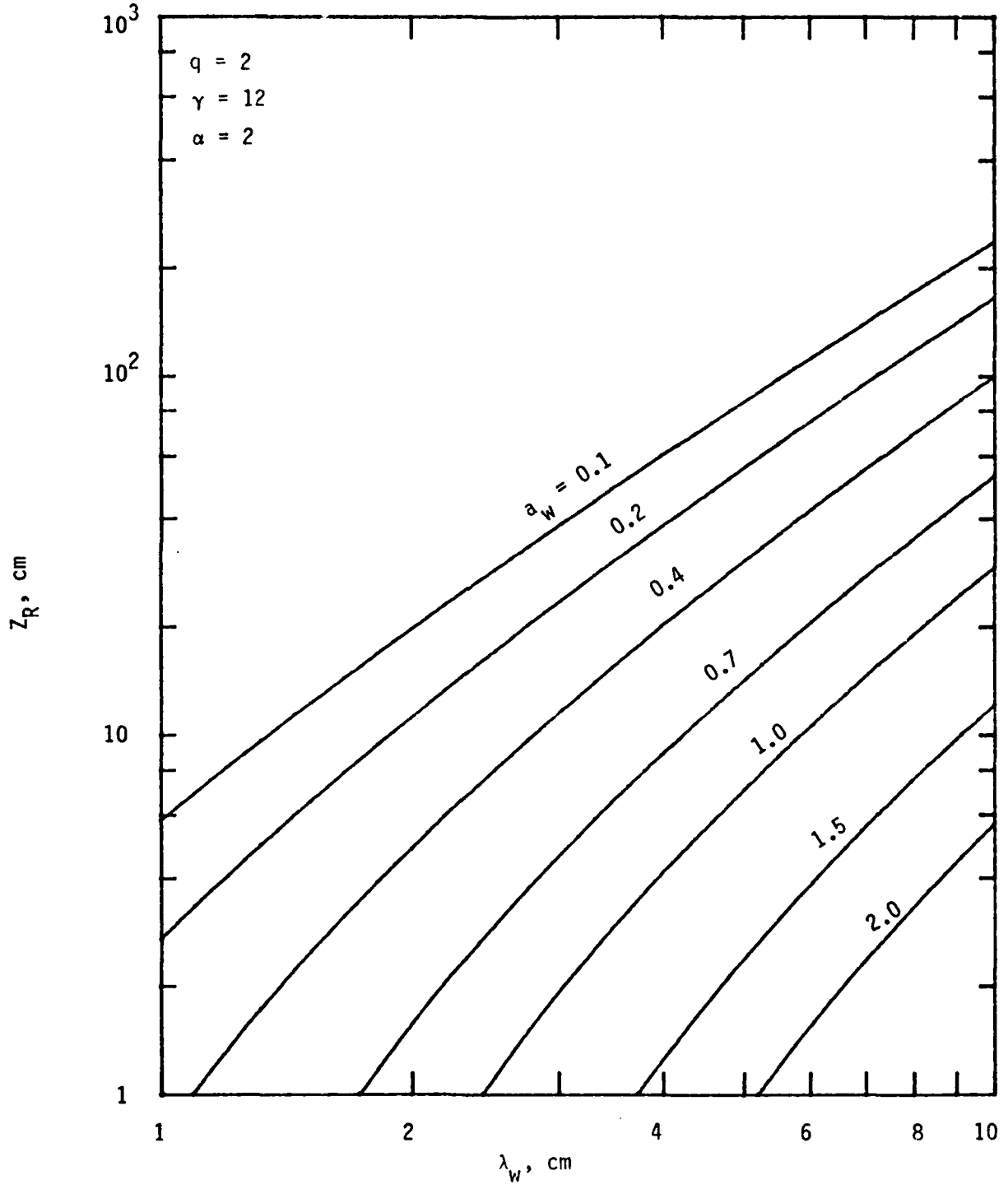

Figure 10. Map of Constant a_w Lines

$$\frac{g_o L_w}{I} = 8.70 \times 10^{-3} \left(\frac{a_w Z_R q}{\lambda_w} \right)^2 \left(\frac{q}{\gamma} \right) / \text{ amp} \qquad (4.7)$$

where I is the total electron beam current. The saturation flux for a constant parameter wiggler is given by

$$\phi_{sat} \simeq 2.67 \times 10^7 \left(\frac{\gamma}{q} \right)^4 \frac{\lambda_w^2}{a_w^2 Z_R^4} \qquad (4.8)$$

For a given set of λ_w and Z_R, a_w can be determined from eq. (4.4). Using eqs. (4.7) and (4.8), we can then find the small signal gain and the saturation flux. Figures (11) to 16) show contours of constant $g_o L_w$, ϕ_{sat} and output wavelength plots for q = 1 and q = 2. In all the cases the magnet gap to optical beam diameter at entrance and exit to the wiggler was taken to be equal to 2. For the UCSB experiment, the same electron beam is planned to be used for the second stage also. Thus, if we fix γ at 12 and pick the first stage parameters, the second stage output wavelength is predetermined. These are also indicated in Figure (16). Now we are in a position to specify the parameters for the proposed UCSB two stage experiment. The Van de Graaff generator is expected to provide 10 amperes current. The bandwidth requirement on the pump wave to be a coherent wave for the second stage is that $\Delta\lambda/\lambda \sim 10^{-4}$. The spontaneous emission from the magnetic wiggler is given by[15]

$$\frac{dI(\omega)}{d\Omega} = 2.94 \times 10^{-8} \cdot h\nu_{ev} \cdot i_{ma} \cdot N \text{ watts/ev of bandwidth /ma/milliradian}^2\text{/cm} \qquad (4.9)$$

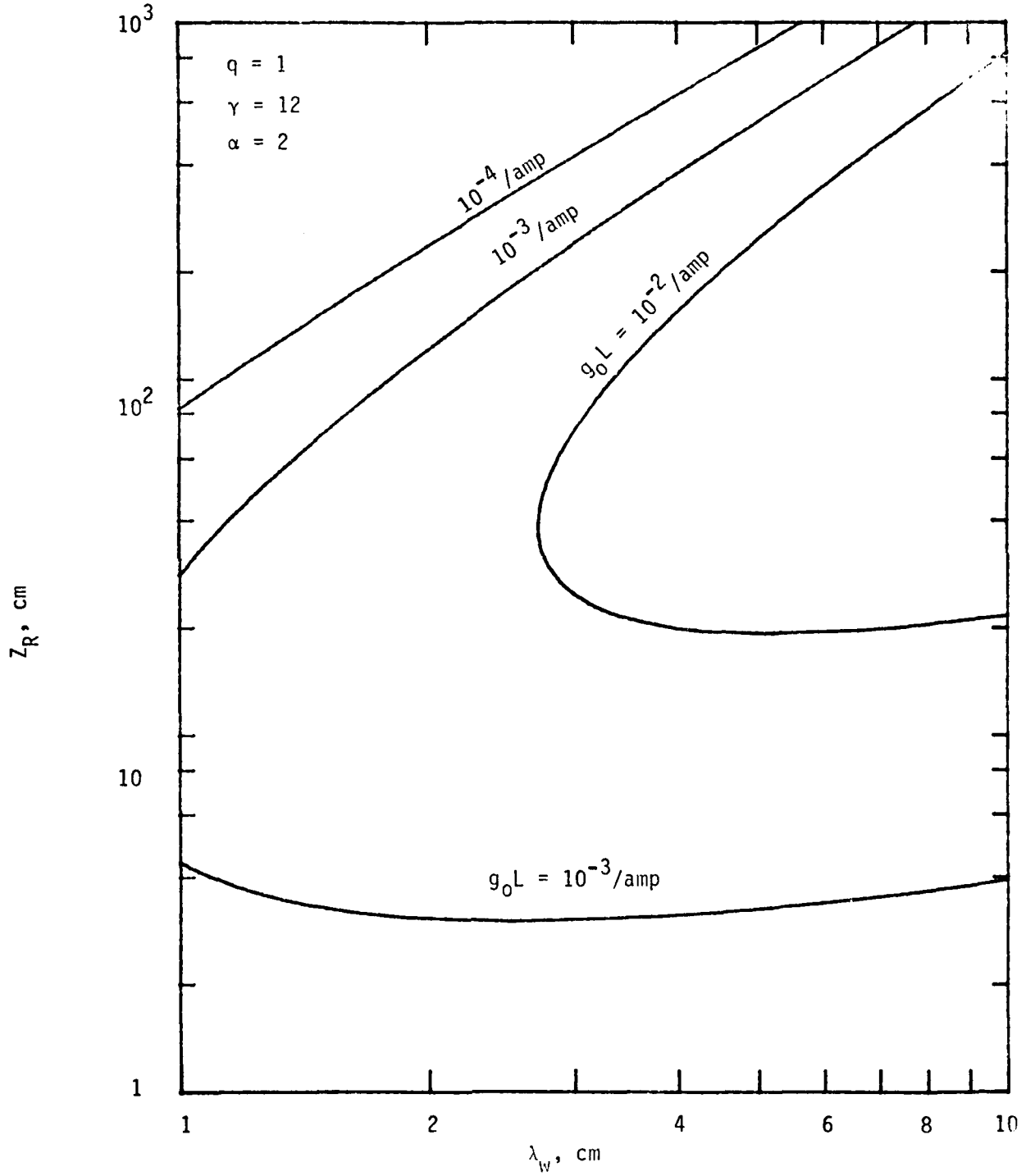

Figure 11. Map of Constant Small Signal Gain Contours for Wiggler Length Equal to Twice the Rayleigh Range

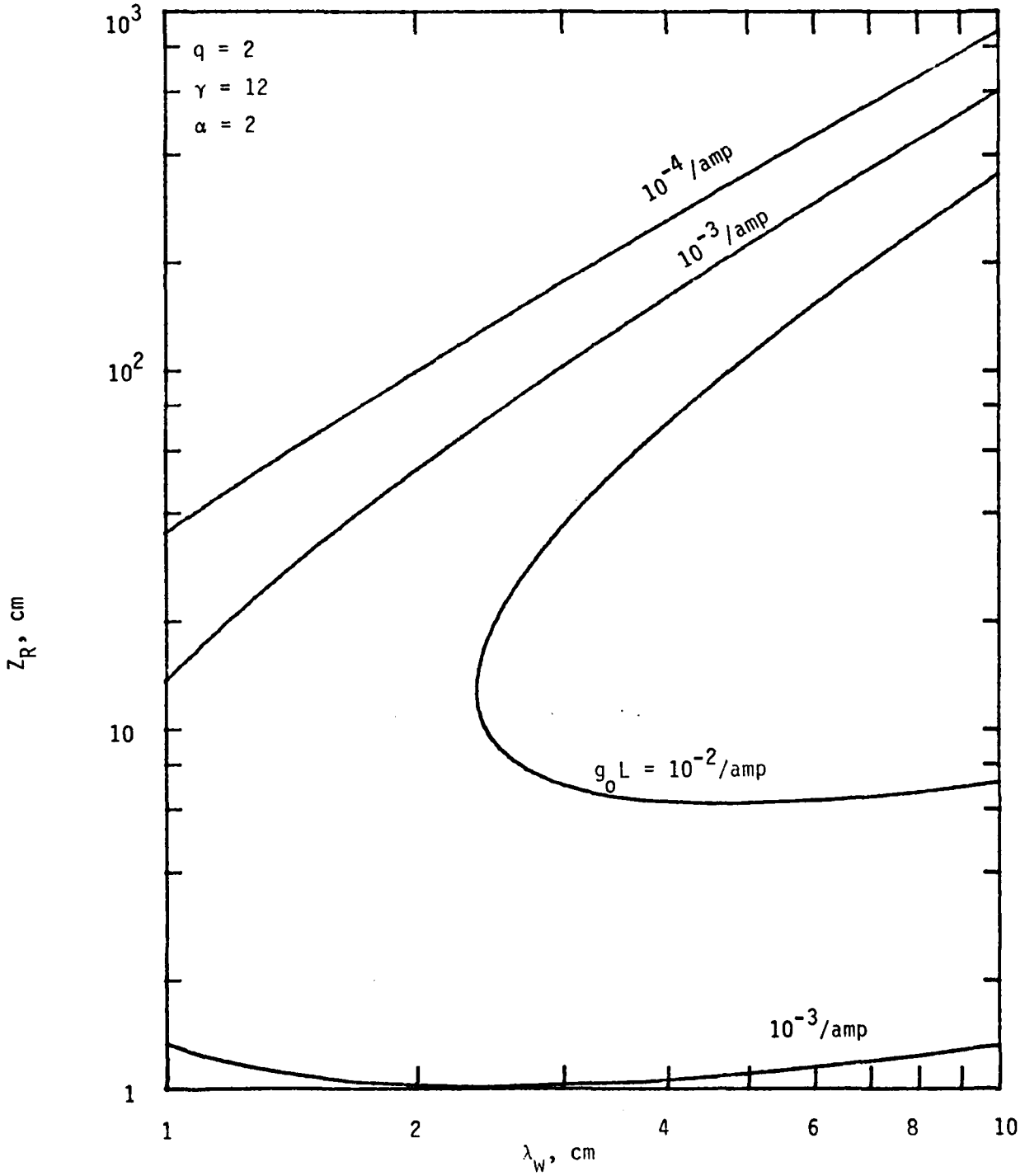

Figure 12. Map of Constant Small Signal Gain Contours for Wiggler Length Equal to Four Times the Rayleigh Range

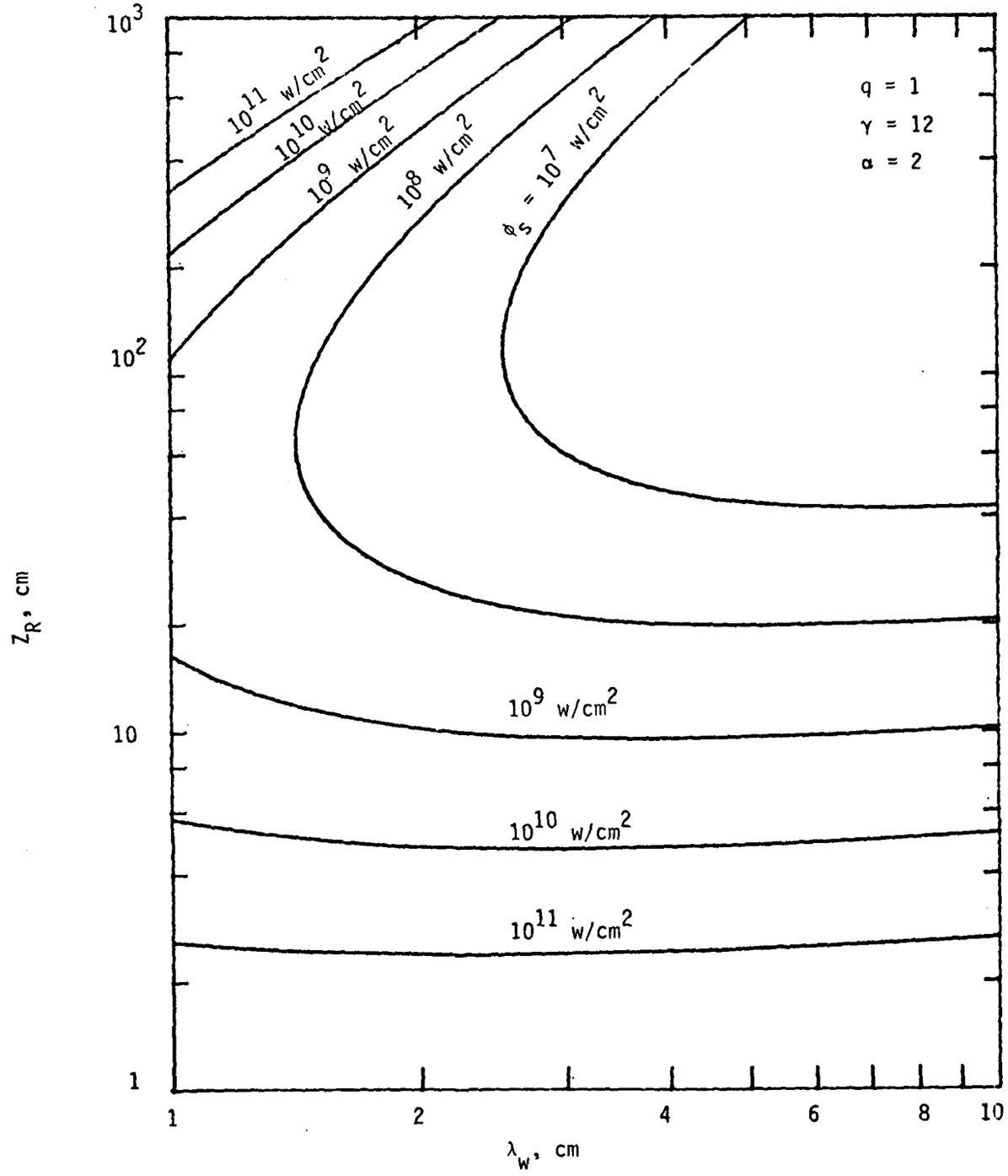

Figure 13. Saturation Flux Contours for $L_W = 2Z_R$

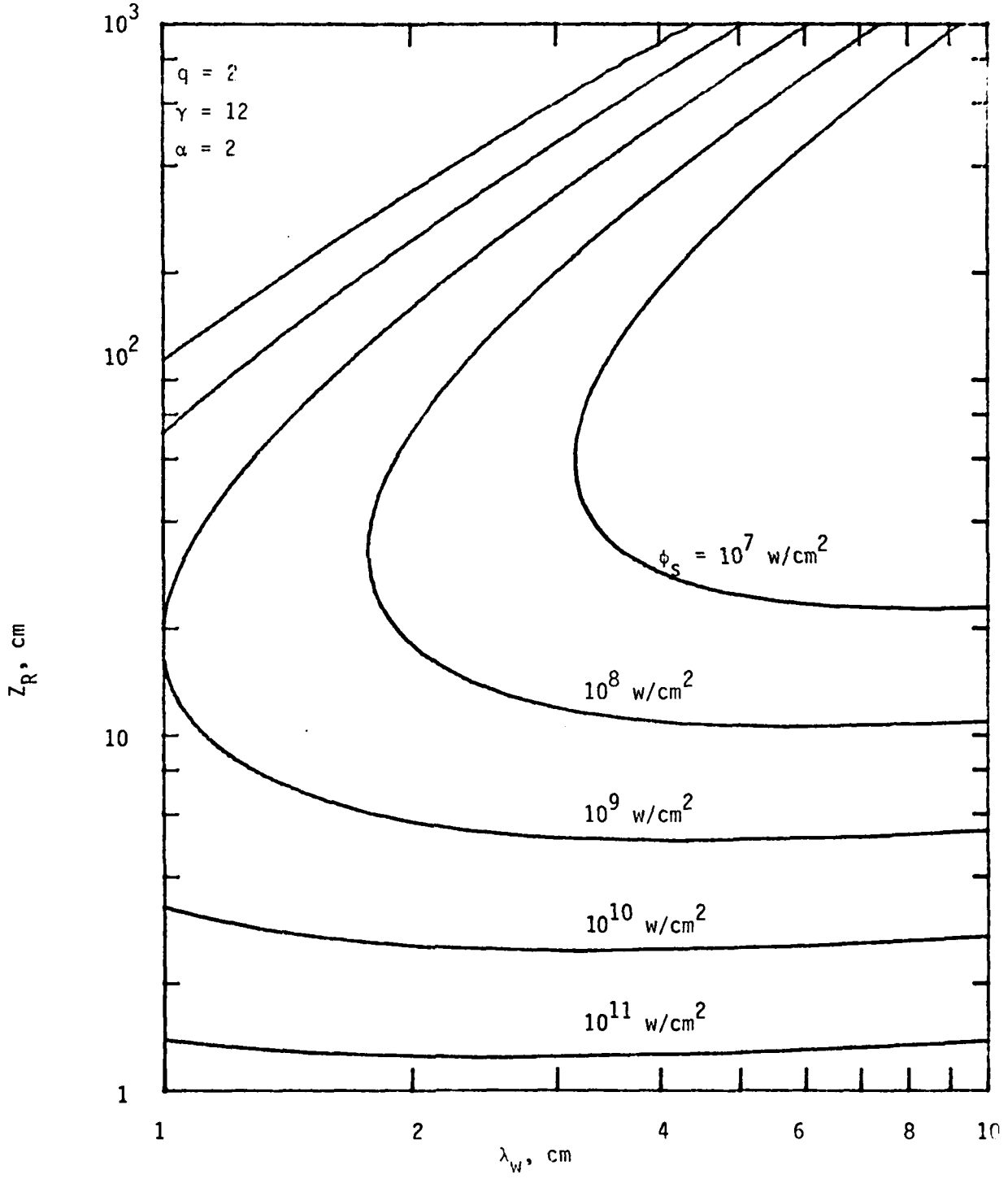

Figure 14. Saturation Flux Contours for $L_W = 4Z_R$

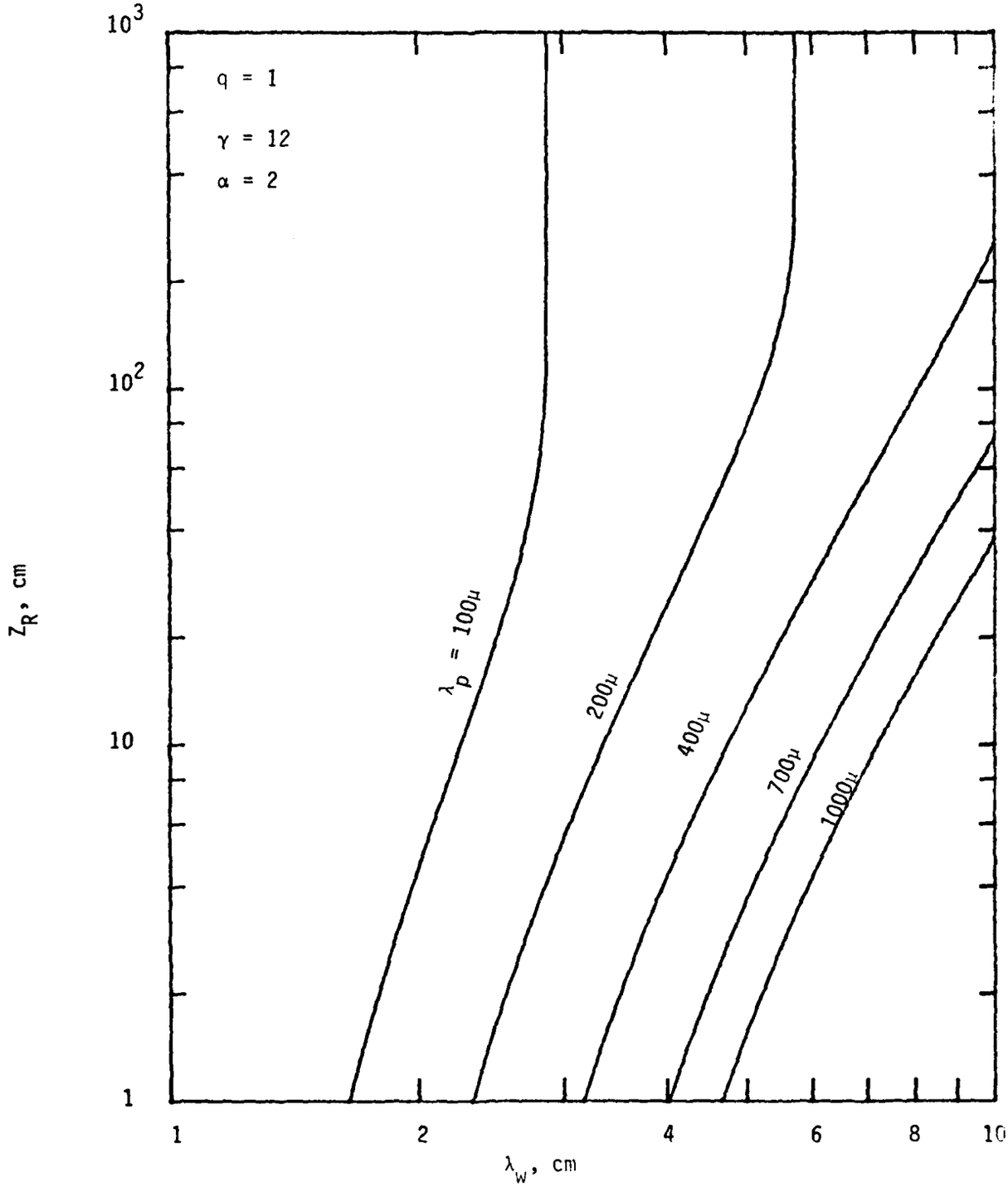

Figure 15. Output Wavelength of the First Stage FEL for $L_W = 2Z_R$

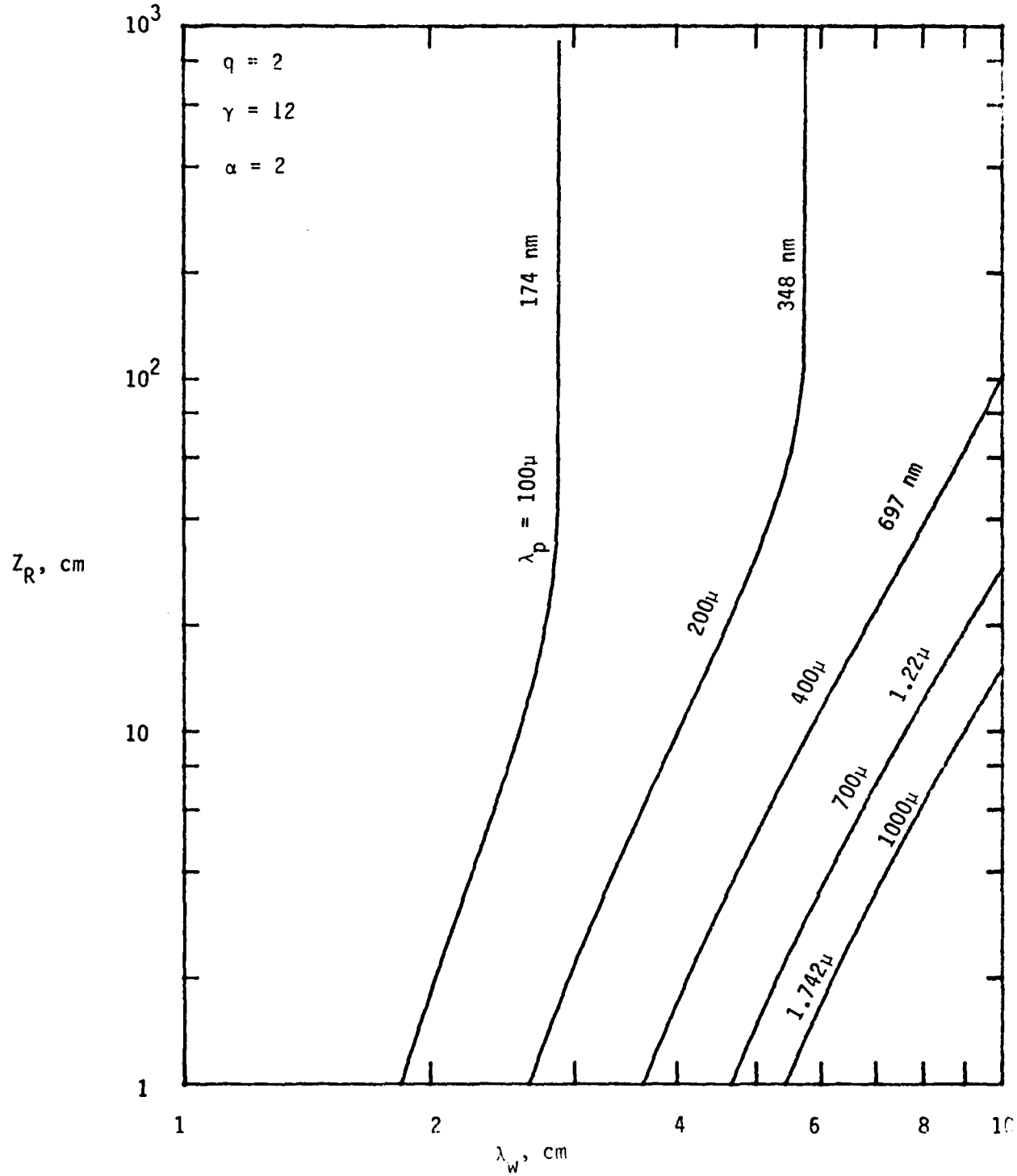

Figure 16. Output Wavelength of the First and Second Stages for $L_W = 4Z_R$

For a pump wavelength of 230μ and N = 5, the spontaneous intensity within the bandwidth of interest is found to be ~ 6.7×10^{-8} watts/cm^2. One would need ~ 35 exponentiations to get to saturation levels of 10^8 to 10^9 w/cm^2.

In Figure (17) we have plotted, once again, lines of constant gain, cavity flux, output pump wavelength and a_w in λ_w-Z_R plane. For γ = 12, the pump wavelength is limited to 230 to 460μ if we stipulate that the output wavelength is in the visible (4000 to 8000 A°). One would also need a small signal gain of at least 5% per pass (requiring ~ 700 passes for saturation). This is important as it directly impacts on the pulse length necessary for a successful two stage operation. From the point of view of wiggler fabrication, one would want to keep $a_w \leq 1$. To achieve reasonable second stage gain, we should have the cavity flux greater than ~ 10^8 w/cm^2. The shaded area in Figure (17) indicates the available parameter space for operation. The actual point that one would pick in this region depends on the pulse length of the electron beam available. If we take the cavity length to be ~ 3 meters, one round trip time is 20 nsec. Thus for 700 passes, the pulse length necessary is 14 μsec. To reduce the pulse length, we have to pick an operating point with higher small signal gain at the expense of decreasing saturation flux. This would reduce the second stage gain and so we cannot arbitrarily increase the small signal gain. We can, however, locate the first stage interaction region away from the beam waist and hope to operate the second stage interaction region at the beam waist. Usually, the advantage gained by such tricks is not overwhelming. If we choose $g_o L_W$ to be 10% per pass (for 10 ampere current), then for a 3 meter cavity, we would need ~ 7 μsec long pulse

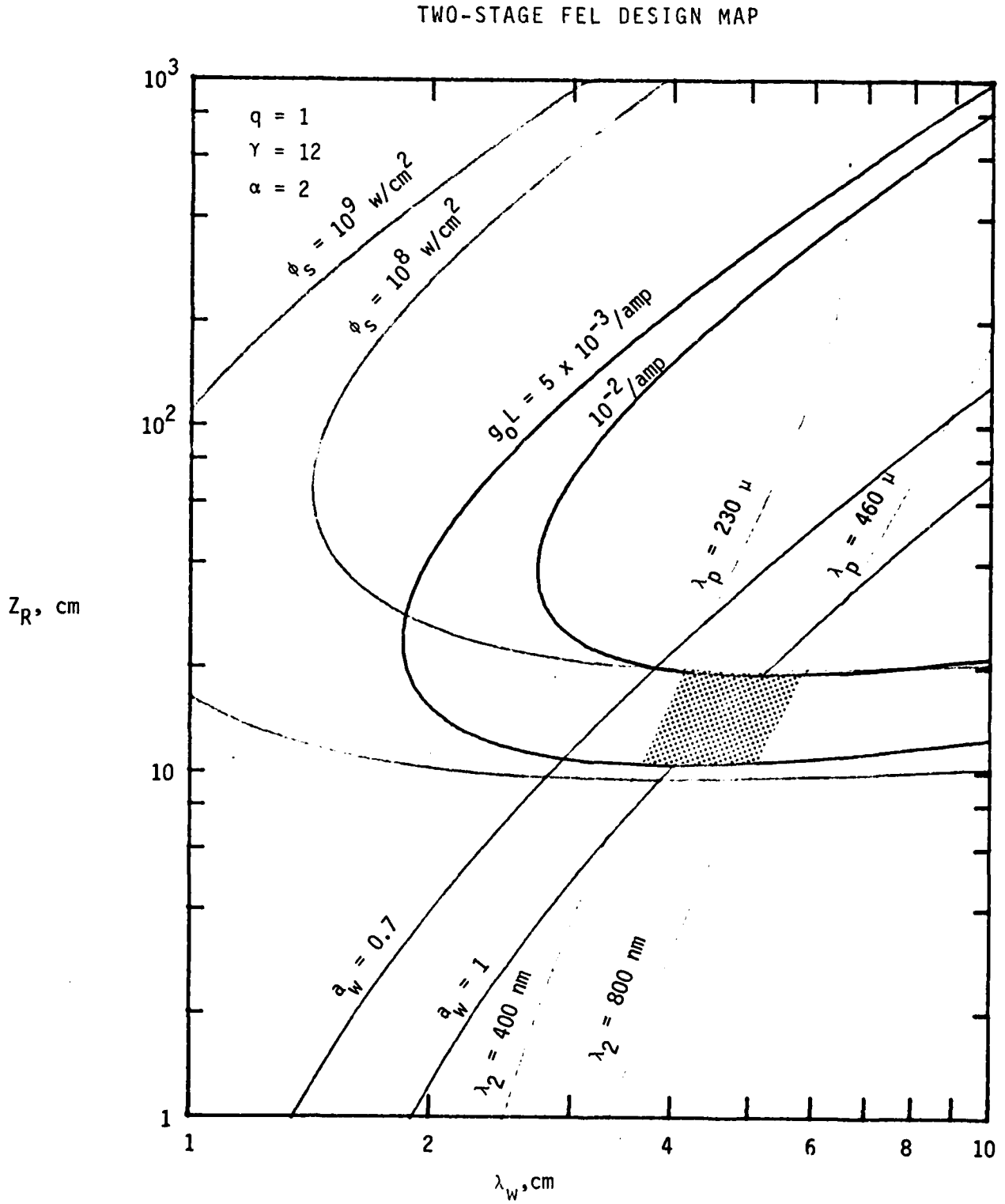

Figure 17. Two-Stage FEL Design Map for γ=12 and $L_W = 2Z_R$

(neglecting optical losses). A 2 meter cavity would reduce this to ~ 5 μsec. Figures (18) to (20) show similar plots as Figure (17) but for different values of q and γ. Using these figures, we can pick a conceptual design point for the operation of the two stage FEL. It must be borne in mind that the boxed region's boundary is somewhat fuzzy and arbitrary. The requirement on the output wavelength can be considerably relaxed if one uses two separate electron beam sources for the first and second stage. The limit on the minimum gain/amp can be relaxed if the current can be increased to say 100 mperes. Comparing Figures (17) and (18), we see that q = 2 gives a bigger operating window than q = 1. One does not want to arbitrarily increase q and operate with a smaller Rayleigh range because (a) the photon beam size at the waist would approach the pump wavelength and (b) the formulas we have used here assumed sensibily constant flux over the length of the wiggler and therefore would not be applicable. For the conceptual design of the two stage FEL, we would therefore choose the nominal parameter values given in Table IV for the UCSB experiment.

For a 10 μsec long pulse, the fluence at the beam waist is ~ 6 KJ/cm^2. An area expansion of ~ 100 would bring the mirror fluence to 60 J/cm^2 and energy absorbed with 0.2% absorption would be ~ 120 mj/ cm^2, which should be quite safe interns of mirror damage. If L_c is the length of the optical cavity and R_1 and R_2 are the mirror radii, we can define quantities g_1 and g_2 by

$$g_{1,2} = 1 - L/R_{1,2} \qquad (4.10)$$

For stability[16], we require that $0 < g_1 g_2 < 1$. We shall consider the symmetric case with $g_1 = g_2 = g$. Since we want the beam to expand rapidly, we shall choose a design where the cavity is nearly concentric ($L \simeq 2R$).

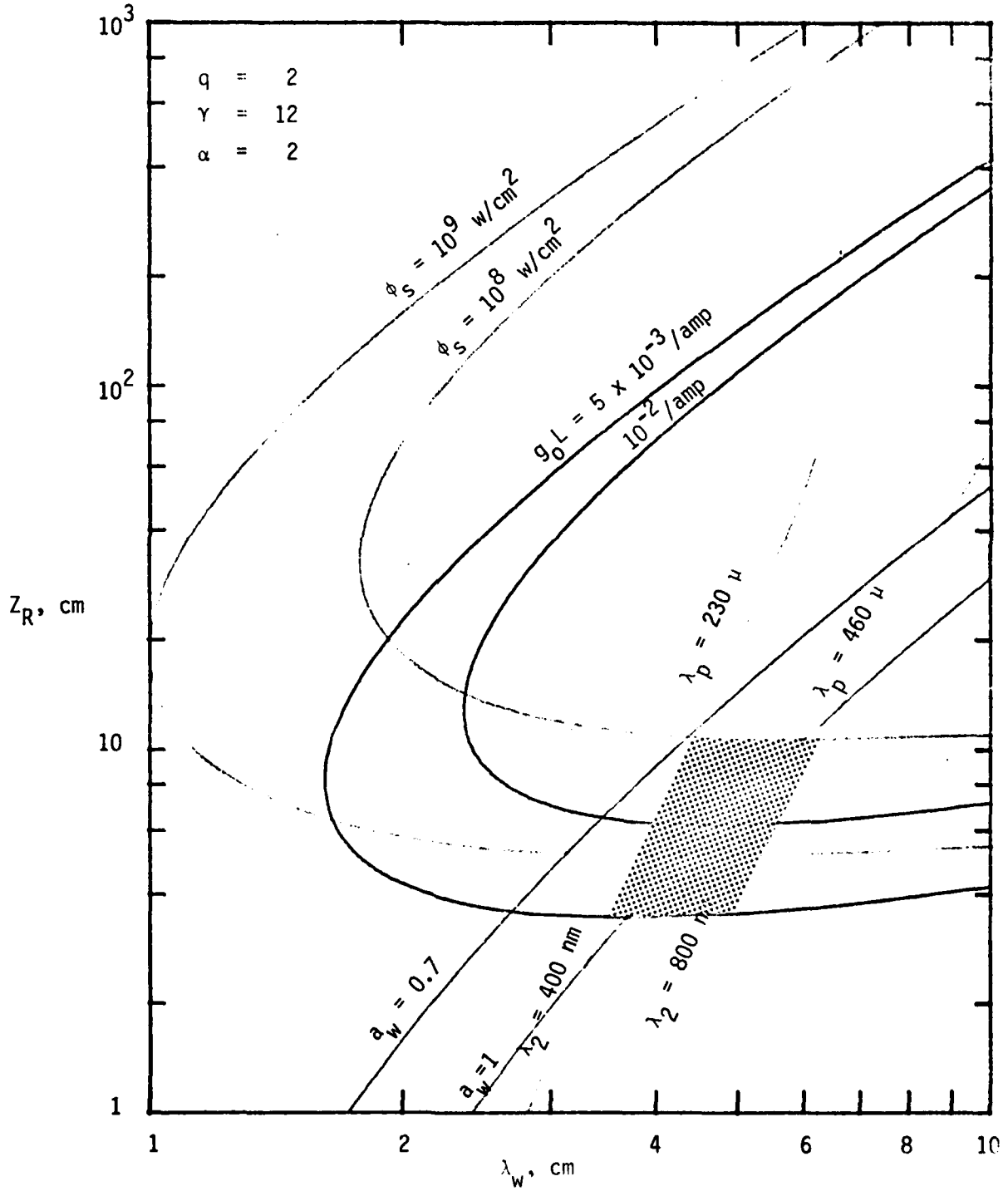

Figure 18. Two-Stage FEL Design Map for γ=12 and $L_W = 4Z_R$

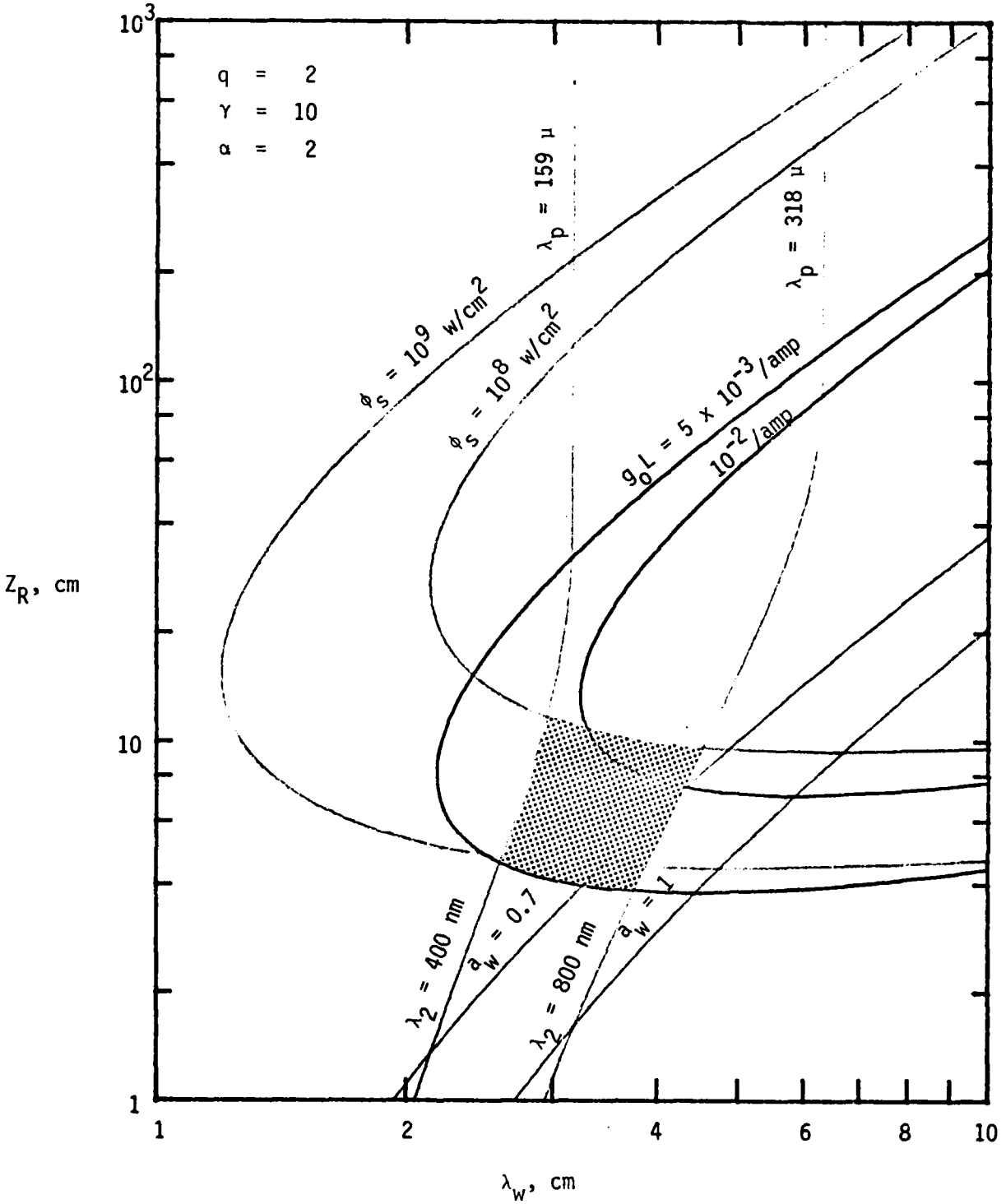

Figure 19. Two-Stage FEL Design Map for γ=10 and $L_W = 2Z_R$

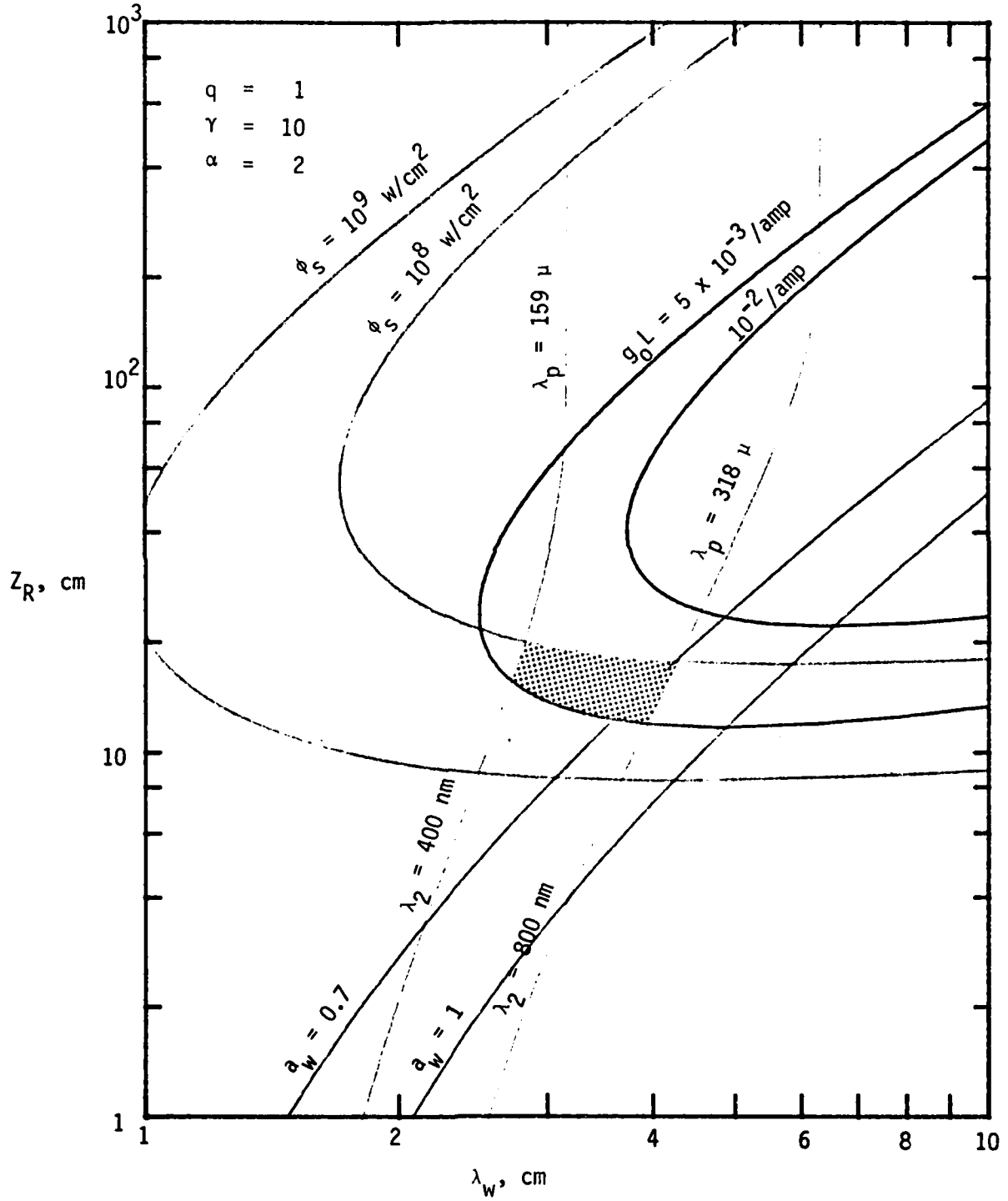

Figure 20. Two-Stage FEL Design Map for γ=10 and $L_W = 4Z_R$

TABLE IV

WIGGLER PARAMETERS FOR THE TWO-STAGE FEL EXPERIMENT

γ	=	12
I	=	10 amp
λ_w	=	4 cm
Z_R	=	6 cm
L_W	=	24 cm
a_W	=	0.855
$g_o L_W$	=	9.54% per pass
ϕ_s	=	5.8×10^8 w/cm^2
w_o	=	2.14 mm
λ_p	=	240 μ
λ_s	=	419 nm

Number of periods = 6

Let $L/R = 2 - \varepsilon$. Then

$g = \varepsilon - 1$.

The radius of the beam at the waist is given by [16]

$$w_o = \left(\frac{\lambda L_c}{\pi} \right)^{1/2} \frac{\left[g_1 g_2 (1 - g_1 g_2) \right]^{1/4}}{\left[g_1 + g_2 - 2 g_1 g_2 \right]^{1/2}}$$

$$= \left(\frac{\lambda L_c}{2\pi} \right)^{1/2} \left(\frac{\varepsilon}{2-\varepsilon} \right)^{1/4} \qquad (4.11)$$

Equation (4.11) can be rewritten as

$$\pi w_o^2 = \frac{\lambda Z_R}{2} \frac{L_c}{Z_R} \left(\frac{\varepsilon}{2-\varepsilon} \right)^{1/2} \qquad (4.12)$$

Since Z_R is defined to be $\pi w_o^2/\lambda$, we have,

$$q_c \left[\varepsilon/(2-\varepsilon) \right]^{1/2} = 2 \qquad (4.13)$$

where $q_c = L_c/Z_R$.

The spot size on the mirrors is given by

$$w_1 = \left(\frac{\lambda L_c}{\pi} \right)^{1/2} \left[\frac{g_2}{g_1 (1 - g_1 g_2)} \right]^{1/4} \qquad (4.14)$$

This can be cast in the form,

$$q_c \left[\frac{1}{\varepsilon (2-\varepsilon)} \right]^{1/2} = w_1^2/w_o^2 \qquad (4.15)$$

From equation (4.13) and (4.15), we obtain,

$$\varepsilon = 2 w_o^2/w_1^2 \qquad (4.16)$$

$$q_c = 2 \left(\frac{2-\varepsilon}{\varepsilon} \right)^{1/2} \qquad (4.17)$$

Knowing q_c and ε, we can obtain the cavity length and mirror radius of curvature. The diameter of the mirror can be calculated by fixing

the diffraction loss. Li[17] has numerically calculated the diffraction losses for different |g| values, and Fresnel numbers. In general, if $|g| < 0.99$, one would need Fresnel number of 15 or larger to keep the diffraction losses per pass to $< 10^{-4}$. In Table V two different cavity designs are given for an area expansion factor of 100 and 200 for a Fresnel number of 15 ($= a^2/\lambda L_c$, where a is the radius of the mirror).

The choice between the first and second design would depend on other factors such as space to bend the electron beam into and out of the wiggler, electron beam pulse length, etc.

TABLE V

OPTICAL CAVITY PARAMETERS

Beam Area Expansion	100	200
ε	0.02	0.01
q_c	19.90	28.21
Cavity Length L_c	119.4 cm	169.3 cm
Radius of Curvature	60.3 cm	85.1 cm
Mirror radius a	6.56 cm	7.81 cm
Pump wavelength	240 μm	240 μm
Cavity Round Trip	~ 8 nsec	~ 11.3 nsec

SECTION V

SUMMARY

We have investigated several methods of reducing the pump cavity losses in a two stage free electron laser. We have found that with metal optics, we can reduce the round trip cavity absorption losses to ~ 0.2% with some difficulty. The cavity wall losses can be significantly decreased by resorting to superconducting optics. The limitations of this system is that the operating wavelength has to be a few millimeters and the operating temperature has to be < 2°K to keep the refrigeration power at a reasonable level. One has also to pay the price of the complexity of the system. For near term UCSB experiment, it was felt that room temperature silver coated optics would be the best choice. To expand the optical beam to low flux levels that the mirrors can handle, it was necessary to use near concentric resonator geometry. For such a configuration, the diffraction losses could be maintained $<10^{-4}$ by choosing Fresnel number greater than or equal to 15. $< .0001$

A permanent magnet Samarium Cobalt wiggler configuration was chosen for the optimization of the wiggler design procedure. We found that all the key parameters for a successful design of the two stage FEL could be mapped in the convenient parameter space of wiggler period and Rayleigh range of the pump photon beam. By overlaying the several parameters such as small signal gain per pass, saturation flux, output wavelength etc. in the same parameter space, we were able to identify a region for the operation of the first stage of the two stage FEL. This enabled us to pick a reasonable set of FEL parameters for the first stage. Knowing the beam waist radius and saturation flux, we could

calculate the spot size on the mirror and expansion needed to handle the optical flux. This in turn enabled us to obtain the cavity length and mirror radii of curvature. Using a Fresnel number of 15, we finally obtained the mirror size.

Detailed analytical calculations have to be carried out to calculate saturation flux and other parameters correctly. This in turn would impact on the optical cavity design slightly. The optimization procedure discussed gives a range of design parameters (albeit narrow) for a given output wavelength. Further optimization may be carried out depending on the applications requirements, etc.

REFERENCES

1. S. A. Mani and T. Naff; Study of Free Electron Laser for Navy Applications; WJSA-FR-80-57 (1980) (C).
2. F. W. French, T. Naff and S. A. Mani; Low voltage Free Electron Laser, Vol. I - Applications Analysis; Report 81S-WA-035, June 1981 (S)
3. S.A. Mani and C. S. Chang; Low Voltage Free Electron Laser, Vol. II-Theory; Report WJSA-FTR-81-168, June 1981.
4. J. D. Jackson, "Classical Electrodynamics," (John Wiley and Sons, Inc, New York), 1975, p. 339.
5. Harold Fetterman, M.I.T. Lincoln Lab, private communication.
6. W. W. Mumford, Proceedings of the IRE, 49, 427 (1961).
7. J. F. Carlson and A.E . Heins, Quarterly of Applied Mathematics, 4, 313 (1947).
8. A. E. Heins and J. F. Carlson, Quarterly of Applied Mathematics, 5, 82 (1948).
9. B. S. Chandrasekhar in "The Encyclopedia of Physics," 2nd Edition, Van Nostrand Reinhold Co., 1974, pp. 904-908.
10. H. Pfister, Cryogenics, January 1976, pp. 17-24.
11. M. A. Allen, Z. D. Farkas, H. A. Hogg, E. W. Hoyt, and P. B. Wilson, IEEE Transaction of Nuclear Science 18, 168 (1971).
12. P. B. Wilson, Z. D. Farkas, H. A. Hogg and E. W. Hoyt, IEEE Transactions of Nuclear Science 22, 104 (1975).
13. TRW Proposal No. 38485-000 R1, "Free Electron Laser Development, Vol. 1, Technical," October 1981, prepared for Office of Naval Research.

14. L. Elias, W. Fairbank, J. Madey, H. A. Schwettman, and T. Smith, Phys. Rev. Letters 36, 717 (1976).

15. B. M. Kincaid, J. Appl. Phys. 48, 2684 (1977).

16. H. Weichell and L. S. Pedrotti, Electro-optical Systems Design, July 1976, p. 21.

17. T. Li, Bell System Tech. J. 44, 917 (1965).